

**DEVELOPMENT OF TURMERIC OIL-LOADED FOLIC  
ACID-GRAFTED CHITOSAN/ALGINATE  
NANOCAPSULES FOR TARGETED DELIVERY TO  
BREAST CANCER**



A Thesis Submitted in Partial Fulfillment of the Requirements  
for the Degree of Master of Science in Pharmaceutical Sciences and  
Technology  
Common Course  
FACULTY OF PHARMACEUTICAL SCIENCES  
Chulalongkorn University  
Academic Year 2021  
Copyright of Chulalongkorn University

การพัฒนาอนุภาคนาโนโคโตนาน/อัลจินตที่กราฟต์ด้วยกรดโพลิกที่  
บรรจุน้ำมันหอมระเหยขมิ้นชันเพื่อนำส่งสู่มะเร็งเต้านมอย่างจำเพาะ  
เจาะจง



วิทยานิพนธ์นี้เป็นส่วนหนึ่งของการศึกษาตามหลักสูตรปริญญาวิทยาศา  
ศาสตรมหาบัณฑิต  
สาขาวิชาเภสัชศาสตร์และเทคโนโลยี ไม่สังกัดภาควิชา/เทียบเท่า  
คณะเภสัชศาสตร์ จุฬาลงกรณ์มหาวิทยาลัย  
ปีการศึกษา 2564  
ลิขสิทธิ์ของจุฬาลงกรณ์มหาวิทยาลัย



เทีต เทีต โม ซาน : การพัฒนาอนุภาคนาโนโคโตซาน/อัลจิเนตที่กราฟต์ด้วยกรดโพลิกที่บรรจุน้ำมันหอมระเหยขมิ้นชันเพื่อนำส่งสู่มะเร็งเต้านมอย่างจำเพาะเจาะจง. ( DEVELOPMENT OF TURMERIC OIL-LOADED FOLIC ACID-GRAFTED CHITOSAN/ALGINATE NANOCAPSULES FOR TARGETED DELIVERY TO BREAST CANCER ) อ.ที่ปรึกษาหลัก : รศ. ภก. ดร.พรชัย โรจนลีทธิศักดิ์, อ.ที่ปรึกษาร่วม : รศ. ดร.ปราณี โรจนลีทธิศักดิ์, ศ. ภญ. ดร. โอภา วัชรคุปต์

ตัวรับโฟเลตมีการแสดงออกในมะเร็งหลายชนิด รวมทั้งมะเร็งเต้านม ซึ่งเป็นแนวโน้มกลยุทธ์เป้าหมายของการนำส่งเคมีบำบัด ในการศึกษานี้ได้พัฒนานาโนแคปซูลโคโตซาน/อัลจิเนต คอนจูเกตกับกรดโพลิกที่บรรจุน้ำมันขมิ้นชัน (TO-FA-CS / Alg NC) โดยใช้เทคนิคไออออปิกเจเลชันเพื่อเข้าไปยังเป้าหมายตัวรับโฟเลตในเซลล์มะเร็งชนิด MBA-MB-231 และ MCF-7 การคอนจูเกตของกรดโพลิกกับโคโตซานผ่านอินทรีย์ด้วย <sup>1</sup>H-NMR และ FT-IR การออกแบบบ็อกซ์-เบห์นเคนถูกนำมาใช้ในการปรับสูตรให้เหมาะสม โดย TO-FA-CS / Alg NC ที่ได้ปรับสูตรแล้วให้ขนาดอนุภาคที่เหมาะสมขนาด 189 นาโนเมตร กระจายตัวเป็นเนื้อเดียวกัน ในขณะที่อนุภาคดังกล่าวมีประสิทธิภาพการกักเก็บ เท่ากับ 35.9% และ ความสามารถในการบรรจุยาเท่ากับ 1.82% ผลการศึกษาการปลดปล่อยยาในหลอดทดลองแสดงให้เห็นว่า น้ำมันขมิ้นชันถูกปลดปล่อยแบบเนิ่น ซึ่งเหมาะสำหรับนำไปใช้ในการบริหารยาทั้งโดยการรับประทานและการฉีด นอกจากนี้การทดสอบการอยู่รอดของเซลล์แสดงให้เห็นว่า TO-FA-CS / Alg NC มีความเป็นพิษสูงกว่า TO-CS / Alg NC และ น้ำมันขมิ้นชันที่ไม่ได้บรรจุในแคปซูล เมื่อทดสอบกับเซลล์มะเร็ง MBA-MB-231 และ MCF-7 ที่มีการแสดงออกของตัวรับโฟเลต ผลการทดลองนี้บ่งชี้ว่า FA-CS / Alg NC มีศักยภาพสามารถนำมาพัฒนาเพื่อนำส่งยาขนาดเล็กลงเข้าสู่เซลล์มะเร็งเต้านมที่มีการแสดงออกของตัวรับโฟเลต



สาขาวิชา      เกษษศาสตร์และเทคโนโลยี  
ปีการศึกษา      2564

ลายมือชื่อนิสิต .....  
ลายมือชื่อ อ.ที่ปรึกษาหลัก .....  
ลายมือชื่อ อ.ที่ปรึกษาร่วม .....  
ลายมือชื่อ อ.ที่ปรึกษาร่วม .....

# # 6272003333 : MAJOR PHARMACEUTICAL SCIENCES AND TECHNOLOGY

KEYWORD: Conjugation, folic acid, chitosan, alginate, nanocapsule, turmeric oil, breast cancer

Htet Htet Moe San : DEVELOPMENT OF TURMERIC OIL-LOADED FOLIC ACID-GRAFTED CHITOSAN/ALGINATE NANOCAPSULES FOR TARGETED DELIVERY TO BREAST CANCER . Advisor: Assoc. Prof. Pornchai Rojsitthisak, Ph.D. Co-advisor: Assoc. Prof. Pranee Rojsitthisak, Ph.D., Prof. OPA VAJRAGUPTA, Ph.D.

Folate receptors that are overexpressed in various cancer cells including breast cancers have become a promising strategy in targeted delivery of chemotherapeutics. In this study, the folic acid (FA)-conjugated chitosan/alginate nanocapsules loaded with turmeric oil (TO-FA-CS/Alg NC) were developed by ionotropic gelation technique to target folate receptors in MBA-MB-231 and MCF-7 breast cancer cell lines. The successful conjugation of FA with CS was confirmed with <sup>1</sup>H-NMR and FT-IR, and Box-Behnken design was utilized in optimizing the formulation. The optimized TO-FA-CS/Alg NC rendered suitable particle size (189 nm) with homogenous distribution and high encapsulation efficiency (35.9%) and loading capacity (1.82%). The *in vitro* drug release profile of TO-FA-CS/Alg NCs also showed sustained TO release that is suitable for both oral and parenteral routes of administration. Furthermore, cell viability assay proved that TO-FA-CS/Alg NC had higher cytotoxic effects than TO-CS/Alg NC and unencapsulated TO against MBA-MB-231 and MCF-7 overexpressing folate receptors. These results suggest that the FA-CS/Alg NC can be promising targeted nanocarriers to folate-positive breast cancer cells.



Field of Study:	Pharmaceutical Sciences and Technology	Student's Signature .....
Academic Year:	2021	Advisor's Signature .....
		Co-advisor's Signature .....
		Co-advisor's Signature .....

## ACKNOWLEDGEMENTS

I would like to genuinely thank my dearest advisor, Associate Professor Pornchai Rojsitthisak, for guiding and bringing the best in me throughout the study. Through your guidance, I was able to gain a deeper understanding and appreciation of this novel concept. I would like to express my deepest gratitude to Associate Professor Pranee Rojsitthisak for believing that I am capable of taking on a very challenging, yet ultimately fulfilling study. Thank you for always finding time to respond to my queries despite your very busy schedule. Thank you for always understanding my limitations and excuses, and for encouraging me to go further and do better. Above all, thank you for making me feel comfortable and always welcome whenever I talk to you. I also would like to express my deepest gratitude to Professor Opa Vajragupta, for giving me invaluable pieces of advice in my synthesis whenever something did not go as planned.

I am extremely grateful to the thesis committee for their valuable comments on this thesis.

To my beloved parents and family, words are never enough to express how grateful I am for everything that you have done and sacrificed for me. Thank you for tirelessly accommodating all our requests and demands.

Lastly, thank you to my labmates for your kindness, words of comfort, carefree conversations, and for providing me emotional support and advice. I could not have done everything I was able to accomplish without you. I dedicate every success, every recognition, and every victory to you.

Htet Htet Moe San

# TABLE OF CONTENTS

	<b>Page</b>
ABSTRACT (THAI) .....	iii
ABSTRACT (ENGLISH) .....	iv
ACKNOWLEDGEMENTS .....	v
TABLE OF CONTENTS .....	vi
LIST OF TABLES .....	8
LIST OF FIGURES .....	9
LIST OF ABBREVIATIONS .....	11
CHAPTER 1: INTRODUCTION .....	13
1.1. Background of the study .....	13
1.2. Rationale and significance .....	16
1.3. Objectives of the study .....	20
1.4. Hypothesis .....	20
CHAPTER 2: LITERATURE REVIEW .....	21
2.1. Breast cancer subtypes and treatment strategies.....	21
2.2. Folic acid as a ligand in targeted delivery of bioactive compounds.....	27
2.2.1. Folic acid .....	27
2.2.2. Folate receptors .....	28
2.2.3. Targeted delivery via the folate receptor.....	29
2.2.4. Folic acid-grafted chitosan (FA-CS) .....	31
2.3. Polymeric nanoparticles.....	35
2.3.1. Alginate .....	36
2.3.2. Chitosan.....	37
2.4. Anticancer potential of turmeric oil.....	39
2.5. Conceptual framework .....	41
CHAPTER 3: MATERIALS AND METHODS .....	43

3.1. Chemicals and Instruments.....	43
3.1.1. Chemicals .....	43
3.1.2. Instruments .....	43
3.2. Methodology .....	44
3.2.1. Synthesis of FA-CS.....	44
3.2.1.1. Synthesis of FA NHS-ester .....	44
3.2.1.2. Conjugation of the FA NHS-ester with CS .....	45
3.2.2. Characterization of the FA-CS .....	45
3.2.3. Preparation of TO-FA-CS/Alg NCs .....	46
3.2.4. Optimization of the NC formulation using BBD .....	47
3.2.5. Characterization of the TO-FA-CS/Alg NCs.....	47
3.2.6. Cell culture .....	50
3.2.7. Determination of cell surface folate receptor expression.....	50
3.2.8. Cytotoxicity assay .....	51
3.2.9. Statistical analysis.....	51
CHAPTER 4: RESULTS AND DISCUSSION.....	52
4.1. Synthesis and characterization of FA-CS .....	52
4.2. Assay of <i>ar</i> -turmerone content .....	55
4.3. Model development for particle size, EE, and LC .....	56
4.4. Validation of the response surface model.....	62
4.5. <i>In vitro</i> release kinetics study.....	65
4.6. Folate receptor expression level .....	71
4.7. Cytotoxicity assay .....	71
CHAPTER 5: CONCLUSION .....	75
REFERENCES .....	84
VITA.....	94



## LIST OF TABLES

	<b>Page</b>
Table 1. Folic acid-grafted polymers for targeted cancer therapy .....	19
Table 2. Turmeric oil-loaded chitosan/alginate nanoparticles .....	20
Table 3. FDA-approved drugs for TNBC .....	24
Table 4. Clinical studies involving combination therapy for TNBC .....	25
Table 5. Clinical studies targeting the FR in TNBC .....	26
Table 6. Various chemical substitutions of folate .....	28
Table 7. Folic acid-grafted chitosan nanoparticles incorporating natural compounds for breast cancer therapy .....	33
Table 8. Factors and responses in the BBD .....	47
Table 9. Assignment of <sup>1</sup> H-NMR spectral data of FA-CS conjugate in d6-DMSO ....	55
Table 10. BBD to optimize the TO-FA-CS/Alg NC formulation .....	58
Table 11. Summary of the regression analyses of the responses .....	59
Table 12. Validation of the prediction capability of the RSM models .....	64
Table 13. Release kinetics of TO from TO-FA-CS/Alg NCs .....	69
Table 14. Release kinetics of TO from TO-CS/Alg NCs .....	70
Table 15. Mean IC <sub>50</sub> values of the unencapsulated TO, TO-CS/Alg NCs, and TO-FA- CS/Alg NCs against MDA-MB-231 and MCF-7 cell lines .....	74

## LIST OF FIGURES

	<b>Page</b>
Figure 1. A scheme of the formation of the TO-FA-CS/Alg NC .....	18
Figure 2. Five main molecular subtypes of breast cancer.....	21
Figure 3. Chemical structure of folate .....	27
Figure 4. Summary of FR- $\alpha$ gene expression levels in various types of cancers .....	29
Figure 5. Chemical structure of alginic acid.....	37
Figure 6. Chemical structure of chitosan .....	38
Figure 7. Main components of turmeric oil .....	41
Figure 8. A framework for the creation of the design space for the nanocapsule formulation of turmeric oil and the assessment of the optimized formulation .....	42
Figure 9. Scheme for the synthesis of (A) FA NHS-ester using DCC and NHS in DMSO, 24 h, room temperature; (B) FA-CS using the FA-NHS ester and chitosan solution, 24 h, room temperature .....	53
Figure 10. FT-IR spectra of FA, CS, and FA-CS .....	54
Figure 11. <sup>1</sup> H-NMR spectra of FA-CS, CS, and FA in d <sub>6</sub> -DMSO.....	55
Figure 12. Response surface plots showing the effects of FA-CS/Alg mass ratio (X <sub>1</sub> ), turmeric oil concentration (X <sub>2</sub> ), and poloxamer 407 concentration (X <sub>3</sub> ) on (a-c) particle size (Y <sub>1</sub> ), (d-f) EE (Y <sub>2</sub> ), and (g-i) LC (Y <sub>3</sub> ). .....	62
Figure 13. Physical characteristics of TO-CS/Alg NCs: (A) Size distribution by intensity, (B) Zeta potential distribution, (C and D) TEM images at 50,000 and 100,000x magnification, respectively. ....	65
Figure 14. Percent cumulative release of TO from the unencapsulated TO, TO-FA-CS/Alg NCs, and TO-CS/Alg NCs in (A) pH 7.4 and (B) pH 5.5. ....	68
Figure 15. Folate expression levels in MDA-MB-231 and MCF-7 cell lines .....	71
Figure 16. The viability of (A) MDA-MB-213 and (B) MCF-7 treated with TO (positive control), CS/Alg NC and FA-CS/Alg NC (negative controls), and TO-CS/Alg NC and TO-FA-CS/Alg NC (turmeric oil-loaded nanocapsules) containing different TO concentrations. ....	73

## LIST OF APPENDICES

	<b>Page</b>
Appendix 1. Calibration curve of FA by measuring the absorbance at 363 nm.....	76
Appendix 2. (A) Calibration curve of <i>ar</i> -turmerone, UHPLC condition of (B) <i>ar</i> - turmerone and (C) turmeric oil .....	77
Appendix 3. IR spectrum of FA.....	79
Appendix 4. IR spectrum of CS.....	79
Appendix 5. IR spectrum of FA-CS .....	80
Appendix 6. <sup>1</sup> H-NMR spectrum of FA.....	81
Appendix 7. <sup>1</sup> H-NMR spectrum of CS .....	82
Appendix 8. <sup>1</sup> H-NMR spectrum of FA-CS.....	83

## LIST OF ABBREVIATIONS

BC	Breast cancer
TNBC	Triple-negative breast cancer
FR	Folate receptor
TO	Turmeric oil
<i>Ar</i> -turmerone	Aromatic turmerone
FA	Folic acid
CS	Chitosan
Alg	Alginate
FA-CS	Folic acid-grafted chitosan
NCs	Nanocapsules
NPs	Nanoparticles
TO-FA-CS/Alg	Turmeric oil-loaded folic acid-grafted chitosan/alginate
MW	Molecular weight
UV-Vis	Ultraviolet–visible spectrophotometry
UHPLC	Ultra-High Performance Liquid Chromatography
FT-IR	Fourier-transform infrared spectroscopy
<sup>1</sup> H-NMR	Proton nuclear magnetic resonance
TEM	Transmission electron microscope
DLS	Dynamic light scattering
BBD	Box-Behnken design
RSM	Response surface methodology
DMSO	Dimethyl sulfoxide

NHS	N-hydroxysuccinimide
DCC	N,N'-dicyclohexyl carbodiimide
TEA	Triethylamine
NaOH	Sodium hydroxide
PBS	Phosphate-buffered saline
EDTA	Ethylenediaminetetraacetic acid
DCU	Dicyclohexylurea
DMEM	Dulbecco's modified Eagle's medium
DS	Degree of substitution
EE	Encapsulation efficiency
LC	Loading capacity
nm	Nanometer
$\mu\text{g}$	Microgram
mL	Milliliter
$\mu\text{M}$	Micromolar
IC <sub>50</sub>	Half-maximal inhibitory concentration

## CHAPTER 1: INTRODUCTION

### 1.1. Background of the study

Cancer is the second leading cause of mortality worldwide, with approximately 9.6 million deaths, or one in six deaths, in 2018. Locally, the new incidence rates reported in 2020, liver, lung, breast, colon, and rectal cancers are the most common types of cancer in Thailand (1). Worldwide, breast cancer is the primary lethal disease among women based on The Global Cancer Observatory 2020, with an estimated incidence and mortality rate of 37.8% and 12.7%, respectively (2).

Breast cancer originates from abnormal epithelial cell growth of ducts (85%) or lobules (15%) in the breast's glandular tissue. Breast cancer has two general types: non-invasive (ductal carcinoma in situ and lobular carcinoma in situ) and invasive (invasive ductal carcinoma, invasive lobular carcinoma, Paget's disease of the nipple, inflammatory breast cancer, phyllodes tumors of the breast, locally advanced breast cancer, and metastatic breast cancer). Treatment options include hormonal therapy, radiotherapy, chemotherapy, and surgery. Moreover, breast cancer has three major subtypes based on cellular protein expression: (i) hormone receptor-positive breast cancer, (ii) human epidermal growth factor receptor 2 (HER 2) positive breast cancer, and triple-negative breast cancer (TNBC). Estrogen receptor (ER) or progesterone receptor (PR), expressed on the hormone receptor-positive breast cancer, are treated by endocrine therapy. The treatment of HER2-positive breast cancer involves HER2 targeted therapy. Treatment with chemotherapeutic agents, usually coupled with surgery and radiation therapy, are the only options for TNBC (3, 4). High toxicity, poor specificity, and poor efficacy are the main issues with conventional chemotherapeutic

drugs. Nowadays, the fabrication of drug delivery systems with tumor-targeting properties has become the gateway to overcome these issues. Many studies established that folate receptor alpha (FR  $\alpha$ ), a membrane-bound protein overexpressed on the apical surface of epithelial cells, is a promising biomarker and a therapeutic target for breast cancer (5).

Nanotechnology has revolutionized the platform in specific targeting delivery to breast cancer cells (6). Ligands that can be attached to the surface of the nanoparticles to increase the cellular uptake and improve the therapeutic efficacy include antibodies, transferrin, aptamers, glycyrrheticin, sugars (galactose and mannose), folic acid, and peptides (Arg-Gly-Asp or RGD) (7).

Nano-based carriers such as lipid-based nanoparticles, polymeric nanoparticles, inorganic nanoparticles, bio-inspired nanoparticles, and hybrid nanoparticles have distinctive properties, such as specific targeting of cancerous cells, minimizing the adverse effects, and multi-drug resistance (8). Recently, polymeric nanoparticles have been the primary interest in nano-drug targeting systems. Naturally occurring polymers, such as chitosan and alginate, are attractive because of their biological properties such as non-immunogenicity, biocompatibility, biodegradability, sustained-release property into the bloodstream, or cancerous tissue, and enhanced drug encapsulating efficiency (9, 10).

Turmeric (*Curcuma longa* L.), which belongs to the family Zingiberaceae, has been used as a traditional home remedy, dye, and food additive in Southeast Asia. Curcuminoids, oleoresin, minerals, and vitamins are present in the rhizome of turmeric. *Ar-turmerone*, the primary component of turmeric, has been widely used in

pharmaceutical applications due to its unique activities in addition to antibacterial, anticarcinogenic, antioxidant, antifungal, insect repellent, antimutagenic, and antiplatelet properties. Turmeric oil is unstable under specific environments, volatile, and highly lipophilic (11). Although several pieces of research explored the pharmacological activities of turmeric oil against many diseases, these limitations restrict the development of new therapeutic formulations of turmeric oil (12). Encapsulating turmeric oil within a network of biopolymers can overcome the limitations of hydrophobicity and instability. Lertsutthiwong P., et al. (13) reported overcoming these concerns by encapsulating turmeric oil in the alginate nanoparticles. Unfortunately, it showed low stability at room temperature and poor drug loading. Coating the alginate nanoparticles with cationic chitosan polymer improved the stability and loading of turmeric oil (11).

This study aimed to develop the chemical modification of the carboxyl group of the targeting ligand folic acid with the amino group of chitosan, leading to the encapsulation of turmeric oil in the folic acid-grafted chitosan/alginate nanocapsules (FA-CS/Alg NCs). Folic acid was grafted on the backbone of chitosan using the amination-acylation mechanism. UV-Vis, <sup>1</sup>H-NMR, and FT-IR characterized the resulting grafted polymer. The preparation of turmeric oil-loaded FA-CS/Alg NCs was employed o/w emulsification followed by ionotropic gelation. The optimization of the NCs formulation was performed using the response surface methodology with Box-Behnken design as the experimental design. The hydrodynamic diameter, encapsulation efficiency, and loading capacity be the responses with folic acid-chitosan/alginate mass ratio, turmeric oil concentration, and poloxamer 407 concentration as the factors. In addition, the optimized formulation was investigated in



MDA-MB-231 and MCF-7. The percentage of cell viability was the parameter for the cell assay.

## **1.2. Rationale and significance**

TNBC has been known as the heterogeneous phenotype of breast cancer, which accounts for 10-20% of all invasive breast cancers and has many molecular subtypes. TNBC has neither estrogen nor progesterone nor human epidermal growth factor receptor 2 (HER 2) amplification, remarkably eliminating the response to receptor-based therapies and increasing the likelihood of metastasis (3, 4). Chemotherapy is the primary treatment that may be used either alone or combined with other types of therapies. Conventional chemotherapies suffer multidrug resistance and poor selectivity, which affect cancerous cells and normal cells (14). Nowadays, nanotherapeutic platforms are fabricated to overcome the limitations of chemotherapy. Nanotherapeutic drug delivery systems offer the advantages of providing prolonged shelf-life, multitargeting, incorporating hydrophilic and lipophilic active compounds, flexibility in administration via oral, parenteral, nasal, and transdermal routes, and enhancing the biodistribution of anticancer drugs (15). However, selecting the cancer surface molecular biomarkers is essential for targeted drug delivery. Folic acid has been recognized as a potential ligand for targeting cancerous cells. Folic acid is inexpensive, stable, non-immunogenic, and can couple to the backbone of a polymer. Folic acid grafted with polymeric nanocarriers can be a delivery approach targeting the folate receptors expressed on the surface of cancer cells (Table 1) (16). Chitosan and alginate, natural polysaccharides, have unique biological properties such as biodegradability, biocompatibility, low toxicity, good stability, and extended drug release property.

In particular, chitosan can easily attach with folic acid via hydrogen bonding and van der Waals forces (7).

The formulation involves the formation of a micelle core with the hydrophobic tail of poloxamer oriented with the TO in the center and alginate attached to the surrounding hydrophilic head of poloxamer. The addition of  $\text{CaCl}_2$  promotes the formation of an ionic cross-linking of  $\text{Ca}^{+2}$  ions with the guluronic acid blocks of Alg forming an egg-box structure (17). The cross-linking process promotes gelation which could protect TO and maintain its biological activity (18, 19). The folic acid-grafted chitosan (FA-CS) was added last because the folate ligand should be on the surface of the NP for attachment to the folate receptors on the membrane of cancer cells. The FA-CS dry powder was first dissolved in 2% acetic acid and the pH adjusted to 6.0. At this pH, the primary amine groups of CS and the secondary amine groups of FA are both protonated while the carboxyl groups of FA stay protonated (20). These charge states promote the electrostatic interaction of CS with Alg (Fig. 1). Folic acid binds to the folate receptor and enters the cancerous cells via endocytosis for intracellular drug delivery. Covalently conjugating folic acid with chitosan does not interfere with the folate receptor binding and internalization process (5). Folate receptor has a high affinity for binding protein; thereupon, folic acid-grafted chitosan-based NCs can be taken at low concentration while folate receptor can be acceptable in the target area.

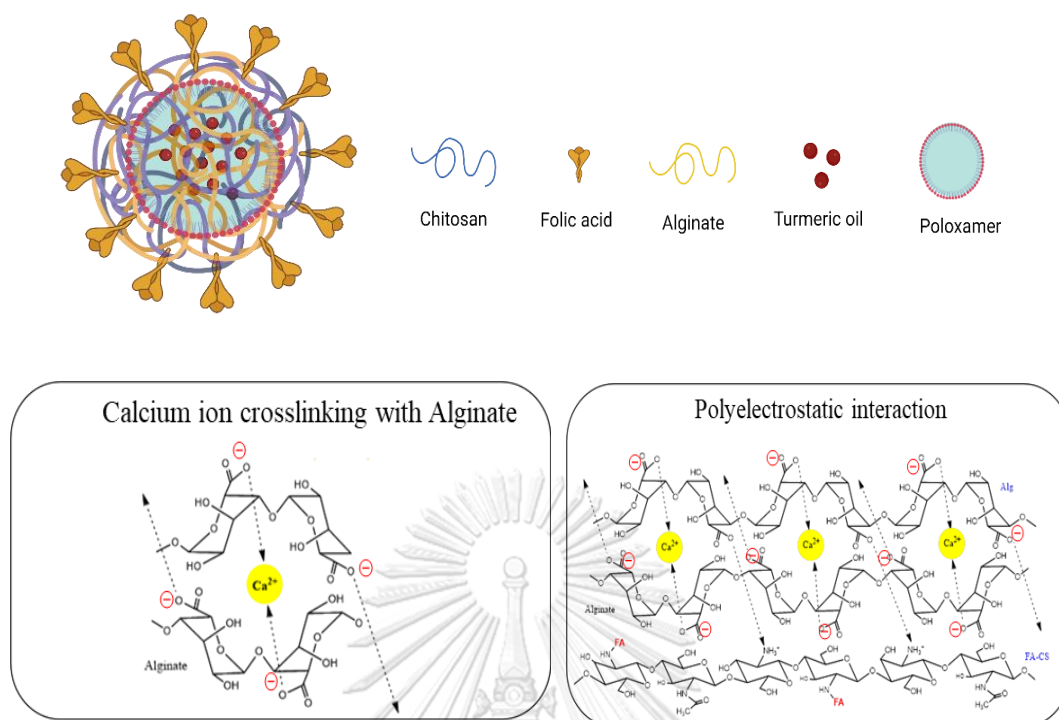


**Figure 1.** A scheme of the formation of the TO-FA-CS/Alg NC

Limited studies show the possibility of encapsulating turmeric oil using chitosan or alginate polymers or combining both polymers (Table 2). However, the use of folic acid as a ligand that can be grafted with chitosan to coat turmeric oil-loaded alginate NCs that intend to target the folate receptors in TNBC cells has not been investigated to date. Moreover, only a few studies have demonstrated the capacity of folic acid-grafted chitosan nanoparticles to increase drug loading capacity, prolong drug release, low cytotoxicity, and cellular uptake (5, 21).

**Table 1.** Folic acid-grafted polymers for targeted cancer therapy

Natural compound	FA-grafted polymer	Type of NP	<i>In-vitro</i> model	Results		References
				Cytotoxic effect	Cellular uptake	
Curcumin	Acrylic polymer	Hydrogel	HeLa (Cervical cancer)	In dose dependent manner (15µM, 25µM, 50µM)	Better cellular uptake than non-folate hydrogel	(22)
Curcumin	Gum acacia	Microsphere	4T1 & MDA-MB-468 (TNBC)	LD <sub>50</sub> of (MDA-MB-468: 45µM, 4T1: 40µM)	More internalized than bare microspheres & curcumin alone	(23)
<i>Helianthus tuberosus</i> extracts	Starch	Copper oxide nanoparticle	MDA-MB-231 (Breast cancer)	IC <sub>50</sub> of NPs (21.03 ± 1.85 µg/mL)	Internalization via endocytosis	(24)
Doxorubicin	Polydopamine	Mesoporous silica nanoparticle	HeLa (Cervical cancer)	Concentration-dependent & time-dependent	1.8-fold higher uptake than non-folate NP	(25)

**Table 2.** Turmeric oil-loaded chitosan/alginate nanoparticles

Polymer used	Type of NP	Method of preparation	Results	References
Sodium alginate (80-120 kDa)	Nanocapsule	Ionotropic gelation method	Particle size ( $116 \pm 14$ nm), zeta potential ( $-24.3 \pm 2.7$ mV), %DL ( $5.47 \pm 0.21$ %)	(13)
Sodium alginate (80-120 kDa) Low MW chitosan (41 kDa) (92±2% DD)	Nanocapsule	Ionotropic gelation method	Particle size ( $522 \pm 15$ to $667 \pm 17$ nm), zeta potential ( $\geq 20$ mV), stable at 4 °C and 25 °C	(11)
Sodium alginate and chitosan	Nanocapsule	Ionotropic gelation method	Particle size (below 300 nm), %EE (71%), slow and sustained release at neutral pH for 48 hours, more antiproliferative properties than free oil in A549 cell lines, hemocompatible	(26)

### 1.3. Objectives of the study

This study aimed to:

- Synthesize and structurally elucidate folic acid-grafted chitosan.
- Optimize and characterize turmeric oil-loaded folic acid grafted chitosan/alginate nanocapsules.
- Evaluate the cytotoxicity of the turmeric oil-loaded folic acid-grafted chitosan/alginate nanocapsules in MDA-MB-231 and MCF-7 breast cancer cell lines.

### 1.4. Hypothesis

This study hypothesized that folic acid-grafted chitosan/alginate nanocapsules as the carrier would enhance the cytotoxicity of turmeric oil against folate-receptor positive MDA-MB-231 and MCF-7 breast cancer cell lines.

## CHAPTER 2: LITERATURE REVIEW

### 2.1. Breast cancer subtypes and treatment strategies

The classification of breast cancer is based on the two types of epithelial cells in the mammary gland: luminal and basal, by immunohistochemically and complementary DNA (cDNA) microarrays. The five subtypes of breast cancer include (i) luminal A (HR +/ HER 2 -), (ii) luminal B (HR +/ HER 2 +), (iii) HER 2 positives, (iv) basal-like (HR/ HER 2 negative, epidermal growth factor receptor-positive and/or cytokeratin 5/6 positive), and (v) normal-like breast cancer (Fig. 2) (4). Basal-like carcinoma is defined as the subtype with neither HR nor HER 2 amplifications. However, expressing the gene on the neoplastic cells found on the basal/ myoepithelial cell of the breast was found to be possible (3). On clinical assay, triple-negative phenotypes enrich basal-like cancer even though 25% of TNBC cases are not basal-like on gene expression array (4).

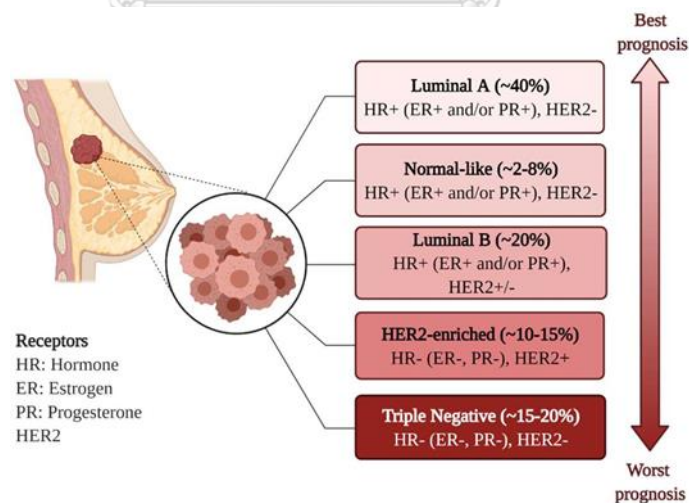


**Figure 2.** Five main molecular subtypes of breast cancer

TNBC accounts for 10-20% of invasive breast cancer, which lacks the overexpression of estrogen/progesterone and HER 2 receptors. However, it expresses the gene proliferation and a unique gene cluster (basal cluster) that comprises epidermal

growth factor receptor (EGFR) and cytokeratins (3). Therefore, patients with TNBC can receive neither targeted therapy against ER/PR/HER2 receptors nor hormonal therapies. Current TNBC treatment modalities involve conventional therapy (neoadjuvant, adjuvant, surgery, radiotherapy), advanced therapy (miRNA, siRNA, aptamers, nanomedicines: quantum dots, fluorescent nano-diamonds, silver NPs, gold NPs, superparamagnetic iron oxide NPs, polymeric NPs) and immunotherapy. Drug delivery via uniquely expressed surface biomarkers on TNBC has been identified to augment the cytotoxicity of the therapeutic payload. Target receptors such as Notch, CD 44, Frizzled (FZD), transferrin, integrin, folate and epidermal growth factor receptor (EGFR) and their signaling pathways can be exploited to induce cell death either by inhibiting cellular proliferation or via cellular apoptosis. Combining chemotherapeutic drugs are the standard and most effective strategy to combat TNBC. FDA has already approved some molecules (Table 3), and some are under investigation in clinical trials (Table 4) (clinicaltrials.gov).

Among these, the folate ligand has been revolutionized due to its participation in the natural progression of cancer cells and its high affinity towards FR. Moreover, there is a higher expression of FRs (especially the  $\alpha$ -isoform) in breast cancer cells compared to normal cells. Therefore, these receptors can be utilized to develop FR-mediated targeted therapy for breast cancer. Investigations in clinical trials have also shown the interest in using this target in chemotherapy (Table 5) (clinicaltrials.gov).

Chemo-active substances may be natural, semi-synthetic, or synthetic. Limited solubility, toxicity toward normal cells, and multi-drug resistance are among the issues

with conventional small-molecule chemotherapeutic agents. These issues lead to low biodistribution and require a high drug concentration to reach the desired site (14, 15).

Over the few decades, NCs platforms have been invented to overcome the challenges with conventional chemotherapeutic agents (15). Nanocarriers of chemotherapeutic drugs are advantageous due to their capacity to load both hydrophilic and hydrophobic drugs, improve pharmacokinetic and pharmacodynamic profiles, exhibit sustained release, increase circulation time and drug concentration, and enhance internalization by the enhanced permeation and retention effect (EPR) or via endocytosis mechanism (27). Among the remarkable properties of nanotherapeutics include their small size and surface, which allow functionalization. Additionally, nanocarriers with an average range of 10-100 nm effectively transport the drug and accomplish the EPR effect (6). In literature revealed that when the polymer was functionalized with folic acid used as a targeting ligand, not only increased the encapsulation efficiency (EE) and loading capacity (LC) of hydrophobic compounds loaded in the NPs but also definitely enhanced the cellular uptake folate receptor-mediated pathway through folic acid targeting. Bolla PK., et al. (134) showed that lutein content was significantly higher when FA conjugated with polymeric nanoparticle. Moreover, cellular uptake was 1.6 and 2-fold enhanced than unconjugated NPs and unencapsulated compound. Furthermore, doxorubicin, hydrophobic drug, was loaded with a high loading capacity into FA conjugated CS (FA-CS) NPs by a combination ionic bonding and hydrophobic effect with Pluronic F127. EE was increased from 35.2% to 58.1% occurring in the FA-conjugated NPs and more cel uptake by folate-receptor mediated endocytosis (124).



**Table 3.** FDA-approved drugs for TNBC

<b>Drug</b>	<b>Route of administration</b>	<b>Mechanism</b>	<b>Trade Name</b>	<b>Year of First Approval</b>	<b>References</b>
Sacituzumab Govitecan-hziy (Antibody-drug conjugate)	IV infusion	The antibody component binds to a specific protein on the surface of cancer cells (Trop-2). The chemotherapy drug called SN-38 is released and kills the cancer cell.	Trodelyv	Apr 2020	(28)
Olaparib (Small molecule)	Oral	PARP inhibitors (poly ADP ribose polymerase, an enzyme involved in DNA repair) work by blocking a protein used to repair damage to DNA that occurs during cell division.	Lynparza	Jan 2018	(29)
Talazoparib (Small molecule)	Oral		Talzenna	Oct 2018	(30)
Atezolizumab (Monoclonal antibody)	IV infusion	Blocks the interaction of PD-L1 (programmed death-ligand 1) with its receptor programmed cell death protein 1 (PD-1) and CD80 receptors (B7-1Rs)	Tecentriq	Mar 2019	(31)

**Table 4.** Clinical studies involving combination therapy for TNBC

Intervention/ treatments	Pharmacologic class	Phase	Condition or Disease	Identifier	Parameters of interest in the study
Drug: Temsirolimus Neratinib Drug: Neratinib	Temsirolimus (mTOR inhibitors) Neratinib (tyrosine kinase inhibitor)	I/II	Metastatic HER2-Amplified disease or TNBC	NCT01111825	Efficacy and safety of combination therapy in advanced breast carcinoma.
Biological: Durvalumab Drug: Olaparib	Olaparib (PARP inhibitor), Durvalumab (immune therapy)	I	Metastasis TNBC	NCT03544125	Efficacy of combination therapy in metastatic breast cancer.
Biological: Mirvetuximab Soravtansine	Antibody-drug conjugate	II	Metastatic FR $\alpha$ (+) TNBC	NCT03106077	Targeted combination therapy of antibody-drug conjugate to FR $\alpha$ .
Drug: Rucaparib Drug: Cisplatin	A small-molecule inhibitor of poly (ADP-ribose) polymerase (PARP) 1,2 and 3	II	TNBC	NCT01074970	Efficacy of combination therapy in TNBC with BRCA1/2 mutations by the inhibition PARP.
Drug: PF-05212384 (gedatolisib) Drug: Docetaxel Drug: Cisplatin Drug: Dacomitinib	PI3K/mTOR inhibitor	I	Neoplasm	NCT01920061	Safety and tolerability of gedatolisib in patients with advanced solid tumors in combination with other antitumor agents.
Drug: SHR-1210 Drug: Apatinib	SHR-1210 (Anti-PD-1 Antibody) Apatinib (VEGFR2 inhibitor)	II	Advanced TNBC	NCT03394287	Efficacy of combination therapy for advanced TNBC.

**Table 5.** Clinical studies targeting the FR in TNBC

<b>Intervention/ Treatment</b>	<b>Details of the study</b>	<b>Identifier, Phase, and Status</b>
<p>Drug: Cyclophosphamide</p> <p>Biological: Low/ high dose FR<math>\alpha</math> vaccine</p>	<p>Objective: Safety evaluation and immunogenicity of two doses of the FR<math>\alpha</math> peptide vaccine with GM-CSF as a vaccine adjuvant, with or without cyclophosphamide.</p> <p>Outcome: No results posted as of December 2021.</p>	<ul style="list-style-type: none"> <li>• NCT02593227</li> <li>• Phase 2</li> <li>• Completed (19 July 2021)</li> </ul>
<p>Biological: Mirvetuximab</p> <p>Soravtansine</p>	<p>Objective: To determine if mirvetuximab as a single agent can induce response in at least 20% of patients with metastatic FR<math>\alpha</math> (+) TNBC.</p> <p>Outcome: The study did not achieve the required number of participants to determine if 20% of patients had a response to mirvetuximab. However, the study reveal that the drug had no serious adverse events occurred during the course of the study.</p>	<ul style="list-style-type: none"> <li>• NCT03106077</li> <li>• Phase 2</li> <li>• Completed (2 Dec 2020)</li> </ul>
<p>Drug: Cyclophosphamide</p> <p>Biological: Multi-epitope FR<math>\alpha</math> Peptide Vaccine with Sargramostim</p>	<p>Objective: To prove that the multi-epitope FR<math>\alpha</math> peptide vaccine with sargramostim as adjuvant will prolong the disease-free survival (DFS) compared to GM-CSF treated TNBC patients.</p>	<ul style="list-style-type: none"> <li>• NCT03012100</li> <li>• Phase 2</li> <li>• Recruiting (30 June 2021)</li> </ul>
<p>Drug: Gemcitabine</p> <p>Hydrochloride</p> <p>Biological: Mirvetuximab</p> <p>Soravtansine</p>	<p>Objective: To determine the maximum tolerated dose (MTD) and the recommended phase 2 dose (RP2D) of gemcitabine in combination with mirvetuximab in FR<math>\alpha</math> (+) cancers.</p>	<ul style="list-style-type: none"> <li>• NCT02996825</li> <li>• Phase 1</li> <li>• Recruiting (26 Jan 2021)</li> </ul>
<p>Drug: ELU001</p> <p>Folic acid-functionalized C'Dot -Drug-Conjugate</p>	<p>Objective: To determine the MTD and RP2D of ELU001 IV infusion in patients with FR<math>\alpha</math> (+) tumors.</p>	<ul style="list-style-type: none"> <li>• NCT05001282</li> <li>• Phase 1,2</li> <li>• Recruiting (3 Dec 2021)</li> </ul>

## 2.2. Folic acid as a ligand in targeted delivery of bioactive compounds

### 2.2.1. Folic acid

Folate has three structural components: a pteridine (2-amino-4-hydroxypteridine) moiety that can be oxidized or reduced, a para-aminobenzoic acid (PABA), and a variable polyglutamic chain (Fig. 3). Folate in nature can either be reduced or oxidized (32).

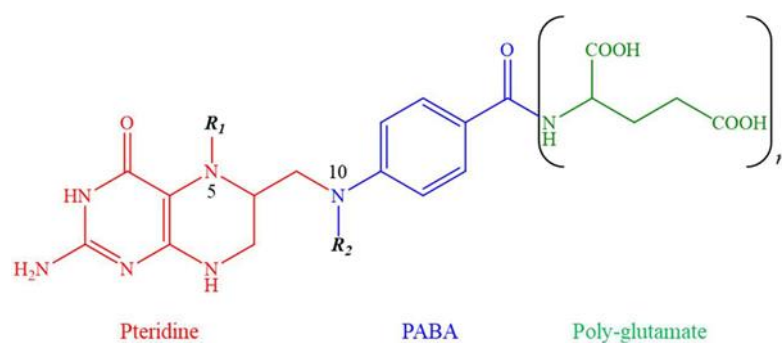


**Figure 3.** Chemical structure of folate

The commonly reduced moiety of natural folate is dihydrofolate (DHF) and tetrahydrofolate (THF) that can be one-carbon substituted in the position of N5 of pteridine ring and N10 of PABA to form 5,10-methyl THF, 5-methyl THF, 5-formyl THF, and 5,10-formyl THF (Table 6). The unsubstituted reduced forms are chemically unstable due to the rapid cleavage of the methylene linker between the pteridine ring and PABA, leading to the inactivation of its biological activities (33). The synthetic folate compound is more stable than naturally occurring folate in food sources that are susceptible to losing their biochemical activities by heat, oxidation, and light during the harvesting, storage, processing, and preparation (34).

**Table 6.** Various chemical substitutions of folate

Folate derivative	N5	N10
tetrahydrofolate (THF)	-H	-H
5-methyl THF	-CH <sub>3</sub>	-H
5,10-methylene THF	-CH <sub>2</sub> -	-CH <sub>2</sub> -
5-10-methenyl THF	-CH=N-	-CH=N-
5-formyl THF	-CHO	-H
10-formyl THF	-H	-CHO
10-formimino THF	-H	-HCNH

Folic acid exhibits unique properties as low immunogenicity, stable storage condition, and a targeted ligand by conjugation with macromolecules that internalize into the FR + cells not only cancers but also inflammatory diseases (35).

### 2.2.2. Folate receptors

Folate receptors belong to the family of high-affinity glycosyl phosphatidyl inositol (GPI) proteins that folate receptor  $\alpha$ ,  $\beta$ ,  $\gamma$ , and  $\delta$  (16). Folate receptor- $\alpha$  is overexpressed on the epithelial layer of solid tumors such as TNBC. However, folate receptor- $\beta$  overexpress in non-epithelial tumors, e.g., acute myeloid leukemia. Folate receptor  $\gamma$  is restricted to malignancies of hematopoietic origin involving lymphoid cells. However, folate receptor  $\beta$  has an absence of affinity to bind with folic acid or folate derivatives (5).

Recent studies on molecular simulation and docking explained how the folate binds to folate-receptor alpha (FR $\alpha$ ) (Fig. 4) (36). FR $\alpha$  is composed of 4 long  $\alpha$ -helices ( $\alpha$ 1,  $\alpha$ 2,  $\alpha$ 3,  $\alpha$ 6), 2 short  $\alpha$ -helices ( $\alpha$ 4 and  $\alpha$ 5) and 4 short  $\beta$  strands ( $\beta$ 1-4). According to the simulation study, the folate binds onto the folate receptor that is perpendicular to

the plane of  $\alpha$ -helices:  $\alpha 1$ ,  $\alpha 2$ ,  $\alpha 3$ . Strong hydrogen bonds and hydrophobic interaction occurred in the pterin ring N and O (N1, N2, N3, N5, and O4) and the carboxyl, hydroxyl, and guanidinium groups of the binding pockets of the FR $\alpha$ . Furthermore, the interaction between the aspartate carboxyl oxygens of FR $\alpha$  and the pterin N1 and N2 nitrogen of folate is associated with its high binding affinity. The simulation study also showed that the glutamate functionalities extend outwards of the binding site, making the carboxylate groups exposed and available for conjugation without affecting its binding affinity to FR $\alpha$  (36).

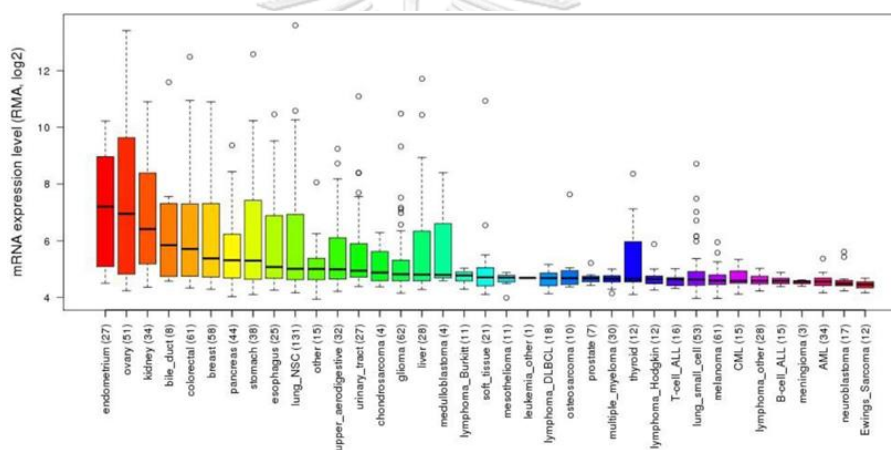


**Figure 4.** Summary of FR- $\alpha$  gene expression levels in various types of cancers

### 2.2.3. Targeted delivery via the folate receptor

Folate receptors are often exploited as targets in cancer therapy for several reasons: (1) they are highly expressed on cancer cells such as ovarian, colon, cervical, breast, lung, kidney, placenta, choroid plexus, and myelogenous leukemias (37); (2) they have a negligible expression in most normal and healthy tissues and organ (38); (3) they have a nanomolar affinity with folate-conjugated drug/ nanoparticles (39); and (4) they induce cellular internalization via receptor-mediated endocytosis and releases the payload into the cell. The delivery of drugs, especially chemotherapeutics via folate-

modified nanoparticles, can be of great advantage compared to the drug itself. This would allow (1) high drug binding and internalization via multivalent folate-conjugate on nanoparticles surface, (2) encapsulation of the drug in a nanocarrier can prevent direct modification of drug, especially when the drug has no modifiable functionalities, (3) delivery of combination drug is possible when encapsulated in a nanocarrier, (4) it can increase the retention in the tumor via EPR effect and facilitate folate receptor-mediated endocytosis, and (5) drug can be protected from biological factors and delay the release until the nanoparticles have been internalized by the cells, hence preventing immediate efflux via multi-drug resistance pumps (16, 40-42).

Receptor-mediated endocytosis happens when a specific ligand binds to its receptor located on the cell surface or the luminal membrane of the blood, brain barrier (BBB) (35). Folate receptor is one of the most common sites for endocytosis, especially cancer-targeting (43). FR-mediated endocytosis takes place in a series of distinct steps (44): (1) first is the interaction and the binding of the folate-conjugate to the FR on the cell surface, (2) then invagination and internalization of the folate-conjugate forming endocytic vesicle occur, and lastly (3) the acidification of the endosomal compartment of pH 5.0 that triggered the gradual release of the folate-conjugate and its payload. The membrane-bound FR are recycled back to the cell surface and allow more folate-conjugates inside the cell. *In vivo* studies revealed that the recycling rate of membrane-bound FR varies from 4 to 12 hours per once cycle (39). It was also found that an insignificant quantity of folate-conjugate enters the lysosome for digestion, thus allowing the delivery of hydrolytically sensitive materials like genes and ribozymes into the cells (45).

#### 2.2.4. Folic acid-grafted chitosan (FA-CS)

Folic acid has low solubility in cold water. Its solubility is improved by increasing the water temperature and changing the solvent pH conditions (acidic or basic). However, they can damage the stability of folic acid (46). Therefore, dimethyl sulfoxide (DMSO) was usually chosen as a solvent for dissolving the folic acid and as the medium for conjugation reactions (47). The carboxy group of folic acid covalently grafted onto the amino group of the chitosan and chitosan derivatives; trimethylated chitosan (TMC) (48), carboxymethylated chitosan (CMC) (49), hydroxypropylated chitosan (HPC) (5, 50), n-octyl-N-phthalyl-3,6-O-(2-hydroxypropyl) chitosan (OPHPC) (51), stearic acid grafted chitosan (52), N-succinyl N'-octyl chitosan (SOCS) (5), octadecyl- quaternized lysine modified chitosan (OQLCS) (42) and, deoxycholic acid-O-carboxymethylated chitosan (DOMC) (53, 54).

The carbodiimide crosslinking reaction is a common reaction for the conjugation of the carboxyl group and primary amino group of polymers via stable amide bond obtaining semi-synthetic polymer (5). FA has been conjugated to the chitosan by "one-plot manner" and "two-step conjugation". The carboxy functional group of folic acid was activated by coupling reagents either 1-ethyl-3-(3- dimethylaminopropyl) carbodiimide (EDC, EDAC, or EDCI) or N, N'- dicyclohexylcarbodiimide (DCC) whether with N-hydroxysuccinimide (NHS) or not. Firstly, the  $\gamma$ -carboxyl group of folic acid reacted with DCC or EDC forming the intermediate O-acylisourea, which is readily hydrolyzed and form N-acyl urea. The addition of NHS can enhance the efficiency of the reaction. The intermediate O- acylisourea reacted with NHS and created the stable NHS ester. After that, the obtained ester reacted with the primary amine of chitosan in



aqueous buffers under the reaction condition of pH lower than 6 and formed the stable amide bond. The conjugation of FA on the chitosan-based nanoparticles to incorporate anticancer drug is exemplified by several studies using carbodiimide reaction and targeting folate-receptor overexpressed breast cancer cell (Table 7).



**Table 7.** Folic acid-grafted chitosan nanoparticles incorporating natural compounds for breast cancer therapy

Natural compounds	Chemicals/ Polymers used	Types of NP	Method of preparation	Outcome of study	In-vitro or In-vivo cytotoxicity study	References
Curcumin	Folic acid, sodium alginate, chitosan (low MW), $\beta$ -cyclodextrin, polyethylene glycol (PEG)	Nanosphere	Ionotropic gelification	Particle size (155 nm)	KMBC-10 (Kerman male breast cancer) cells	(55)
Curcumin (CUR), 5-fluorouracil (5-FU)	Folic acid, chitosan, ferric trichloride hexahydrate, zinc acetate dihydrate (Zn(OAc) <sub>2</sub> ·2H <sub>2</sub> O)	Magnetic bio-metal-organic framework nanocomposite	-	Particle size (48–100 nm), zeta potential (from -9.56 mV to +5.31 mV), PDI (0.2)	MDA-MB-231	(56)
Doxorubicin (DOX)	Folic acid, glycol chitosan (82.7% deacetylated, 250 kDa MW.)	Hypoxia-responsive nanoparticle	Dialysis method	Particle size (674.9 $\pm$ 155.8 nm)	A549 and MCF7, A549 tumor-bearing mice	(57)
Paclitaxel (PTX)	Folic acid, chitosan (>90% deacetylated, 30 kDa MW), deoxycholic acid, EDC, NHS	Micelle	Ultrasonication using a probe-type sonicator	Particle size (126 nm), PDI (0.256), zeta potential (19.37 $\pm$ 2.8 mV)	MCF-7 and H22 (mouse hepatocellular carcinoma cells), H22 xenograft mouse model	(58)
Doxorubicin (DOX)	Folic acid, chitosan (75-85% deacetylated, ~50 kDa MW), DCC,	Nano cochleate	Ethanol injection method and trapping method	Particle size (298 $\pm$ 4 nm), zeta potential (-25.4 $\pm$ 2.4 mV), %EE (74.12 $\pm$ 2.72)	MCF-7	(59)

Ligustrazine (LZ.)	Folate, chitosan, EDC	Nanoparticle	Ionotropic gelation method	Particle size (182.7 ± 0.56 nm), % EE (59.6±0.23), %LC (15.3 ± 0.16)	MCF-7 and A549	(60)
Docetaxel (DTX)	Folic acid, chitosan (low MW), thioglycolic acid (TGA), EDAC, tween 80	Nanoparticle	Ionic gelation method	Particle size (158.50 ± 0.36 nm), PDI (0.36 ± 0.0), zeta potential (+ 18.30 ± 2.52 mV), %EE (71.47 ± 5.62)	MDA-MB-231, Rabbit	(33)
Quercetin (QU)	Folic acid, chitosan, polycaprolactam,	Micelle	-	Particle size (402.65 ± 17.2 nm), zeta potential (-2.58 ± 0.32 mV)	MCF-7 and T-47D, MSC (human mesenchymal stem cell line)	(61)
Curcumin (CUR)	Folic acid, chitosan (89% deacetylated, 400 kDa MW), DCC, NHS, EDC	Nanoparticle	Probe ultrasonication method	Particle size (100–250 nm), zeta potential (-6.55 mV), %EE. (92.06 ± 2.17)	MCF-7 and L929 (non-cancerous cells)	(62)
Camptothecin (CPT) 3,3'-Diindolylmethane (DIM)	Folic acid, chitosan, graphite powder, EDC, NHS	Graphene oxide nano biocomposite	Sonication method	Smoothen and layered surface with proper drug loading	MCF-7, female albino Wistar rats	(63)

### 2.3. Polymeric nanoparticles

Nanoparticles have 5 major classifications based on the type of fabrication methods, including lipid-based nanoparticles (liposome, lipoplex, solid lipid nanoparticles), polymeric nanoparticles (micelle, polymersome, nanocapsule, nanosphere, dendrimer, nanogel, nano complex), inorganic nanoparticles (gold nanoparticles, magnetic nanoparticles, silica nanoparticles, quantum dots, carbon nanomaterial), bio-inspired nanoparticles (exosome, protein nanoparticles, DNA nanostructure) and hybrid nanoparticles (cell membrane-coated nanoparticles, lipid-polymer nanoparticles, organic-inorganic nanocomposite) (64).

Polymeric nanoparticles may constitute the most effective nano vehicles for prolonging anticancer drug delivery in circulation. Nowadays, polymeric nanoparticles have been tested in several preclinical and clinical trials stages. These polymeric nanoparticles can easily be fabricated using biodegradable or non-biodegradable polymers (65). Polymers can be grouped as natural polymers (starch, cellulose, peptide, glycan, protein, alginate, chitosan), synthetic polymers (polylactic acid (PLA), polyethylene glycol (PEG), polycaprolactone (PCL), polyvinyl alcohol (PVA), poly(lactic-co-glycolic acid) (PLGA)) as well as microbial fermentation polymers (polyhydroxybutyrate) (66). Among these natural polymers, cationic chitosan and anionic alginate are remarkable materials in constructing nanoparticles-based vehicles. They have excellent biological properties such as non-toxicity, non-immunogenic, biocompatible, biodegradable, mucoadhesion, adsorption enhancer, hydrophilic, and protective properties (67-70).

### 2.3.1. Alginate

Alginate (Alg) is a water-soluble linear anionic polysaccharide primarily isolated from several brown algae worldwide, such as *Ascophyllum nodosum*, *Laminaria hyperborean*, and *Macrocystis pyrifera* (71). Alg is extracted from algae by mixing with the mineral acid to remove the counterions, such as calcium, magnesium, and sodium, naturally integrated with Alg in seawater. Alginic acid is neutralized by alkalis such as sodium carbonate or sodium hydroxide to produce Sodium Alg (72, 73). Although Alg can be extracted from the bacteria, such as *Pseudomonas* and *Azotobacter* species, these sources are still unavailable for commercial applications (74). Most Alg is commercially above 30,000 metric tons synthesized from farmed brown seaweeds annually (75).

The chemical structure of Alg is composed of  $\beta$ -D-mannuronic acid (M) and  $\alpha$ -L-glucuronic acid (G) residues which are covalently linked by 1,4- glycosidic linkage in different sequences or blocks (76). The block patterns can be composed of consecutive G blocks (G residue) which exhibit rigid and folded structural conformation, consecutive M blocks (M residue) providing flexible and linear conformation, or an alternating G and M block (GM block) (Fig. 5) (76, 77). Compositions and block sequences may vary depending on the isolation of different algae sources (78). Alg has several remarkable polymer properties *in vivo*: good biocompatibility, biodegradability, mucoadhesiveness, pH sensitivity, low toxicity, prolonged circulation time, and gelling properties (79, 80) and can be modified chemically to alter these properties. Alg has been explored as an ideal biomaterial, especially in delivering chemotherapeutic agents (79). The ionic crosslinking of the

carboxylate components of the guluronate moieties on the backbone of Alg with different divalent cations (e.g.,  $\text{Ba}^{2+}$ ,  $\text{Mg}^{2+}$ ,  $\text{Ca}^{2+}$ ) leads to the formation of nanoparticles (81). However, the nanocarriers made from Alg are not stable at room temperature (13). They can easily cause leakage of the active moieties loaded in the core of the nanoparticles (82). Lertsutthiwong P., et al. (11) reported that these limitations could be overcome by coating the Alg nanoparticles with cationic CS biopolymer.

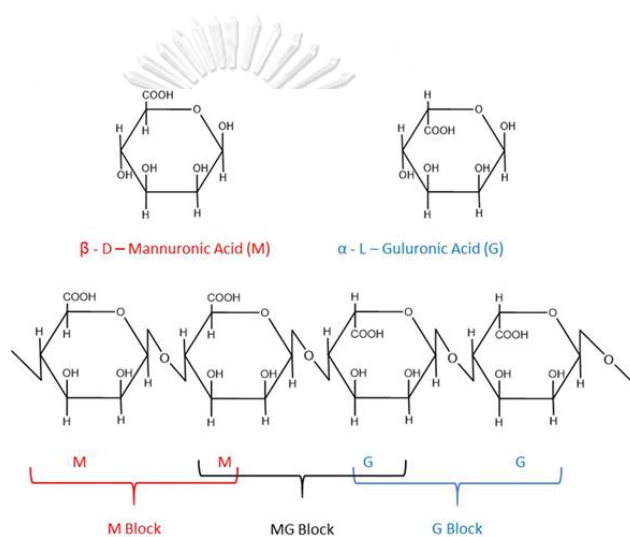


**Figure 5.** Chemical structure of alginic acid

### 2.3.2. Chitosan

Chitosan (CS) is a linear cationic natural polysaccharide, consisting of  $\beta$ -(1 $\rightarrow$ 4) glycosidic linked D-glucosamine and N-acetyl-D-glucosamine (9, 12), is commercially obtained from deacetylation or degradation of chitin which is commonly derived from cell walls of fungi, exoskeletons of insects, and crustacean shells (Fig. 6) (83). Both molecular weight and degree of deacetylation of CS are essential parameters for its physical properties such as degradation, crystallinity, hydrophobicity, and cellular response (84). The human internal enzyme, particularly lysozyme, can

degrade the CS into monosaccharides and oligosaccharides absorbed in the body (85). As mentioned above, Chitosan has unique biological and physicochemical properties: biodegradability, biocompatibility, non-toxicity, mucoadhesiveness, gelling property, membrane permeability, and controlled drug release, which can be fabricated into different forms like beads, films, micro- and nanoparticles. Thus, CS has been utilized in numerous pharmaceutical and medicinal fields, including wound healing, cosmetic production, tissue engineering, drug, vaccine, and gene delivery system (86-88). The free amino ( $-NH_2$ ) and hydroxyl ( $-OH$ ) groups in the CS backbone can be modified to enhance stability and solubility (89).

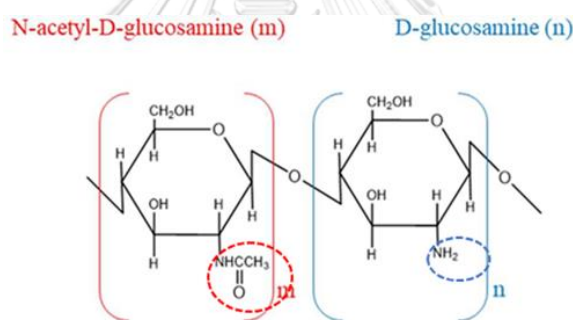


**Figure 6.** Chemical structure of chitosan

The encapsulation of the hydrophobic molecules in the core of the nanoparticles can be done by the interaction of amino groups of polycation CS with the carboxylate groups of polyanion Alg forming a polyelectrolyte complex (PEC) to obtain hydrogel by ionotropic pre-gelation method (12, 90, 91). CS-Alg nanoparticles protect the loaded drug from degradation, sustain the release of the drug, and deliver the drug to the target cell (91). Many researchers have emphasized the fabrication of CS-Alg nanoparticles encapsulating the anticancer compounds and targeting various cancers (90, 92).

#### 2.4. Anticancer potential of turmeric oil

A nutraceutical is a naturally nutrient-rich or medicinally active food or a specific food component that provides medicinal or health benefits, involving the prevention and treatment of several diseases. Among the natural products, turmeric (*Curcuma longa* L.), a rhizomatous herbaceous perennial plant that belongs to the ginger family (Zingiberaceae), has been used as a food additive, nutraceutical, and medicinal products. It is distributed through tropical and subtropical of the world, being widely cultivated in southeast Asiatic countries, mainly in China and India (93).

Turmeric has been widely used as a dye for cloth, cosmetics, and food additives. Turmeric has been well reported for its therapeutic activities to treat several diseases in India and the Chinese system of medicine. Traditional uses of Turmeric include for soothing action in cough and asthma, as a blood purifier, to warm and improve proper metabolism correcting both excesses and deficiencies, to improve digestion, to improve intestinal flora, to relieve gas, to cleanse and strengthen the liver and gallbladder, to normalize menstruation, to eliminate worms, for relief of arthritis and swelling, for local usage on bruises, cuts, burns, insect bites and itches, as antibacterial and anti-fungus (94, 95).

The extract from turmeric powder is about 1-6% curcuminoids, 2-7% dietary fiber, 3-7% dietary minerals, 3-7% essential oils, 5-7% fat, 6-8% proteins, 6-13% water, 60-70% carbohydrates. Phytochemically, at least 235 compounds have been isolated or detected from rhizomes, roots, leaves, and flowers of *Curcuma longa* L., involving 22 diarylheptanoids (commonly known as curcuminoids) and diaryl pentanoids, 8 phenylpropene, vanillic acid, vanillin, 68 monoterpenes, 109 sesquiterpenes, 5



diterpenes, 3 triterpenes, 4 sterols, 2 alkaloids, and 14 other compounds (96, 97).

Essential oils and curcuminoids are principle bioactive components possessing diverse bioactivities *in vitro* and *in vivo* biological assays. Curcuminoids (diarylheptanoids) are mainly accumulated in rhizomes. The essential oils obtained by steam distillation from the rhizomes and roots primarily include sesquiterpenes such as *ar*-turmerone,  $\alpha$ -turmerone, curlone,  $\alpha$ -sesquiphellandrene, zingiberene. The flowers and leaves usually contain monoterpenes such as p-cymene, p-cymen-8-ol, terpinolene (terpinoline),  $\beta$ -phellandrene, myrcene, and cineole. The phytochemical composition of turmeric oils varies in contents with varieties, geographical locations, cultivation conditions, and extraction methods (97).

He XG., et al. (98) identified the major constituents of turmeric oil as *ar*-turmerone,  $\alpha$ -turmerone, and  $\beta$ -turmerone by using GC-MS (Fig. 7). *Ar*-turmerone has been used in pharmaceutical applications because of its biological activities. The chemical structure of *ar*-turmerone is 2-methyl-6-(4-methylphenyl)-2-hepten-4-one), which possess antidepressant (99), antiepileptic (100), antidermatophytic (101), antidiabetic (102), antiplatelet (103), antifungal (104), antibacterial (105), insect repellent (106), antioxidant, antimutagenic (107), anticarcinogenic (108) and immunostimulant (109) activity. However, turmeric oil is a volatile liquid, unstable, and poorly water-soluble, leading to limited progress in its pharmaceutical applications. There are many potential advantages when encapsulating the anticancer drugs in nanoparticles and conjugating with targeted ligands on the surface of nanoparticles, which lead to the targeted delivery and sustained release at the desired sites (26).

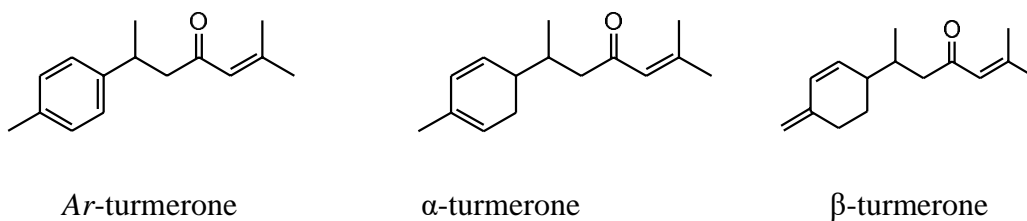


**Figure 7.** Main components of turmeric oil

## 2.5. Conceptual framework

The Box-Behnken design (BBD) of RSM was favorably chosen to establish the design space for developing the optimized formulation. The conditions for the optimum nanoformulation of Turmeric oil were developed by assessing the impact and interaction of the different factors (i.e., FA-CS/Alg mass ratio, turmeric oil concentration, and poloxamer 407 concentration) to the attributes of the nanoformulation (particle size, encapsulation efficiency, and loading capacity).

The response surface methodology established the empirical polynomial equations ( $Y_{\text{pred}} = aX_1 + bX_2 + cX_3 + \dots$ ), which would statistically predict the particle size and loading capacity based on the interplay of the factors (FA-CS/Alg mass ratio, Turmeric oil concentration, and poloxamer 407 concentration). Several parameters have characterized the optimized formulation to ensure applicability as a targeted delivery system.

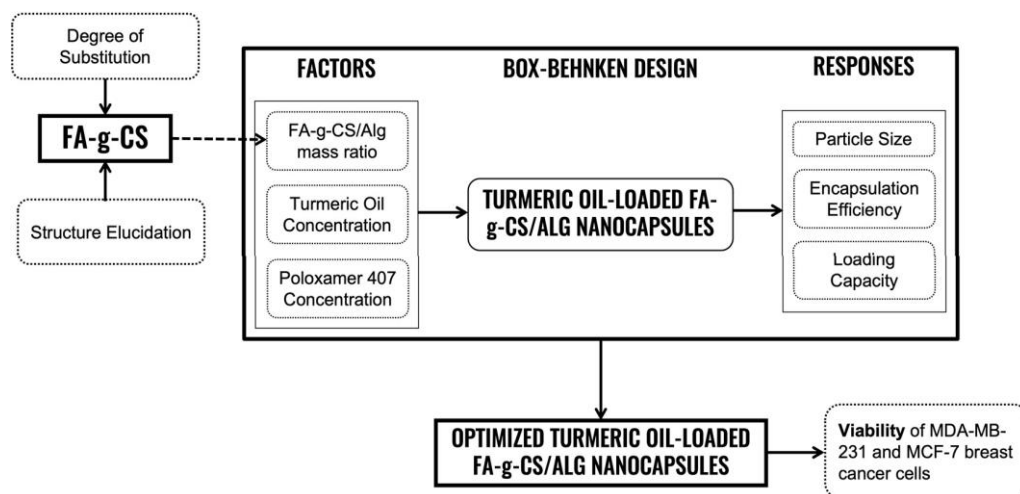


**Figure 8.** A framework for the creation of the design space for the nanocapsule formulation of turmeric oil and the assessment of the optimized formulation



## CHAPTER 3: MATERIALS AND METHODS

### 3.1. Chemicals and Instruments

#### 3.1.1. Chemicals

TO was purchased from TCFE Industry Co., Ltd., Thailand. *Ar*-turmerone was provided by the Department of Chemistry and Center of Excellence for Innovation in Chemistry, Faculty of Science, Ramkhamhaeng University (Bangkok, Thailand). CS (MW = 63 kDa, 91.74% DD) was supplied by Marine Bio-Resources Co., Ltd., (Samut Sakorn, Thailand). Sodium Alg (MW = 120,000 – 190,000 g/mol) and poloxamer 407 were purchased from Sigma-Chemicals (St. Louis, MO). The ratio of mannuronic acid to guluronic acid (M/G ratio) of sodium alginate is 1.56. Folic acid and N, N'-dicyclohexyl carbodiimide (DCC) were purchased from TCI Co., Ltd. (Tokyo, Japan). N-hydroxysuccinimide was supplied from AK Scientific (California, USA). DMSO, acetone, and diethyl ether were purchased from Burdick & Jackson Inc (Michigan, USA). Acetonitrile was purchased from RCI Labscan (Bangkok, Thailand). TEA was purchased from Merck KGaA (Darmstadt, Germany). Absolute ethanol, glacial acetic acid, calcium chloride, and other chemicals were purchased from Carlo Erba reagents (Val de Reuil, France).

#### 3.1.2. Instruments

The following instruments, with their respective models and brands, were provided by the Pharmaceutical Research Instrument Center of the Faculty of Pharmaceutical Sciences: Ultra-High Performance Liquid Chromatography (UHPLC) (Agilent 1290 Infinity II), Intersil<sup>®</sup> ODS- 3 (4.6 x150 mm, 5 $\mu$ ) column, UV-Vis spectrophotometer (Agilent Carry 60), Zetasizer (Malvern Nano ZS, Malvern

Instruments Ltd, UK), ultracentrifuge (Hitachi CP 100NX), incubator shaker (MaxQ6000 shaker), magnetic stirrer with hotplate (Thermolyne, USA), Vortex mixer (Scientific Industries, USA), dialysis regenerated cellulose membrane (MW cut-off 8-14 kDa) (Sigma-Aldrich, USA), analytical balance (Sartorius BA 210S, Germany), lyophilizer (Martin Christ, Germany), microplate reader (Infinite 200 PRO, Tecan Switzerland), confocal fluorescence microscope (Zeiss Apotome). Fourier-transform infrared analysis (PerkinElmer, Spectrum One<sup>®</sup>, CT, USA) was performed at The Scientific and Technological Research Equipment Center, Chulalongkorn University. <sup>1</sup>H-NMR analysis (400 MHz, Bruker Avance DPX-300, CA, USA) was performed at the Faculty of Pharmaceutical Sciences, Chulalongkorn University.

## **3.2. Methodology**

### **3.2.1. Synthesis of FA-CS**

#### **3.2.1.1. Synthesis of FA NHS-ester**

The synthesis of FA ester was based on the procedure described by Alupej L, et al. (114) with slight modification. FA (100 mg) was dissolved in 3 mL of DMSO. After that, 63  $\mu$ L of triethylamine as a catalyst was added to the folic acid solution. Subsequently, DCC and NHS were separately dissolved in DMSO and added a 1:2:2 molar ratio to the carboxyl groups of folic acid. The reaction was performed under a nitrogen atmosphere and stirred overnight in the dark due to the photosensitivity of folic acid.

The initial step for the reaction produced a white precipitate by-product of dicyclohexylurea (DCU). Even though DCU is insoluble in many organic solvents, it can easily be removed by filtration using the 0.2  $\mu$ m syringe filter. Eventually, the

obtained transparent yellow solution was added drop by drop into the cold diethyl ether containing 30 % acetone to initiate the precipitation of the yellow folic acid NHS-ester (FA NHS-ester) product. The precipitate was collected, washed with acetone, and dried under a vacuum desiccator. The final product was stored in the refrigerator for further use.

### 3.2.1.2. Conjugation of the FA NHS-ester with CS

FA-NHS ester solution in DMSO in a 1:3 molar ratio of FA-NHS: CS was slowly added into the CS solution dissolved in acetate buffer (pH was adjusted to 4.5 - 4.7 with 1M NaOH) under continuous stirring in the dark at ambient room temperature. Following 24 h of stirring, the conjugation reaction was stopped by adjusting the pH to 9.0 with 1.0 M NaOH. The solution was purified using a dialysis membrane tube with 8-14 kDa molecular cut-off against PBS (pH 7.4) for 3 days and against deionized water for the next 3 days to remove the unreacted reagents thoroughly. The purified product was lyophilized for 24 h. UV-Vis, <sup>1</sup>H-NMR, and FT-IR have characterized the dried yellow product (110).

### 3.2.2. Characterization of the FA-CS

The folic acid in FA-CS was quantitatively analyzed using a UV-Vis spectrophotometer. Firstly, the calibration curve of standard folic acid in 0.1 M NaOH was prepared with a 2–18 ug/mL concentration range (Appendix 1). Then, 1 mg of FA-CS was dissolved in 10 mL of 2% acetic acid and measured spectrophotometrically at 363 nm (47). The degree of substitution (DS) of FA to CS was computed using the following equations:

$$DS = \frac{\text{Mole of Folic acid}}{\text{Mole of Chitosan}} \quad (1)$$

$$DS = \frac{c/M_{FA}}{(m - c)/M_{\text{Chitosan unit}}} \quad (2)$$

where  $c$  = amount of FA calculated from the calibration curve

$m$  = amount of CS used in this experiment

$M_{FA}$  = molecular weight of FA

$M_{\text{chitosan unit}}$  = molecular weight of CS unit

The chemical composition of CS, FA, and FA-CS was characterized with  $^1\text{H-NMR}$  and FT-IR. The characteristics of FA-CS were analyzed using ATR mode by FT-IR spectrometry in spectral transmittance mode at  $4000\text{-}400\text{ cm}^{-1}$  with a speed of  $4\text{ mm/s}$  and a resolution of  $2\text{ cm}^{-1}$ . The  $^1\text{H-NMR}$  spectrum of FA-CS was run using the deuterated DMSO as a solvent (47).

### 3.2.3. Preparation of TO-FA-CS/Alg NCs

TO-FA-CS/Alg NCs were prepared by emulsifying turmeric oil (oil-in-water emulsion) in sodium Alg aqueous solution followed by ionotropic solution gelation with folic acid-grafted CS using the method described by Lertsutthiwong P., et al. (11) with slight modifications. Briefly, various concentrations (1-2% w/v) of ethanolic turmeric oil solution were added drop by drop into the aqueous Alg solution (20 mL, 0.6 mg/mL) containing varying concentrations (0.5-3% w/v) of poloxamer 407 under continuous stirring (1000 rpm). The o/w emulsion was sonicated for 15 minutes, followed by the addition of calcium chloride solution (4 mL, 0.67 mg/mL). After that, FA-CS solution was added dropwise into the mixture at various concentrations, followed by additional 30 mins stirring (1000 rpm). The turmeric oil-loaded FA-CS/Alg NC suspension was equilibrated overnight in the dark before characterization.

### 3.2.4. Optimization of the NC formulation using BBD

The BBD of RSM was employed to optimize the TO-FA-CS/Alg NCs. In this study, three factors, FA-CS/Alg mass ratio ( $X_1$ ), concentration of TO ( $X_2$ ), and concentration of poloxamer 407 ( $X_3$ ), were investigated in various combinations. These factors and their three levels and the critical attributes of the NCs, namely minimum particle size ( $Y_1$ ) and maximum values for encapsulation efficiency (EE,  $Y_2$ ) and loading capacity (LC,  $Y_3$ ), are summarized in Table 8. The main, interaction, and quadratic effects were expressed in the polynomial equations. Based on the design, 15 experimental runs were required and randomized to exclude any bias.

**Table 8.** Factors and responses in the BBD

Variable	Level		
	Low	Medium	High
Factors			
$X_1$ = FA:CS/Alg mass ratio	0.03:1	0.05:1	0.07:1
$X_2$ = Turmeric oil concentration [% w/v]	1	1.5	2
$X_3$ = Poloxamer 407 concentration [% w/v]	0.5	1.75	3.0
Responses			Constraints
$Y_1$ = Particle size [nm]			Minimum
$Y_2$ = Encapsulation efficiency [%]			Maximum
$Y_3$ = Loading capacity [%]			Maximum

### 3.2.5. Characterization of the TO-FA-CS/Alg NCs

After being equilibrated one night, the nanosuspension was lyophilized and kept in a dry place. However, nanosuspension was used to analyze the zeta size,



encapsulation efficiency and biological assay. The optimized TO-FA-CS/Alg NCs were characterized in terms of the hydrodynamic diameter, polydispersity index, size distribution, zeta potential, and morphology. The dynamic light scattering technique measured the hydrodynamic size and PDI with an angle detection of 90° and the controlled temperature at 25 °C using a Zetasizer. The laser doppler electrophoresis technique determined the zeta potential. Transmission electron microscopy evaluated the size distribution and morphology of the TO-FA-CS/Alg NCs. The encapsulation efficiency and loading capacity of TO-loaded NCs were evaluated using ultrahigh-performance liquid chromatography (UHPLC) with an indirect method according to the study of Lertsutthiwong P, et al. (11) with minor modifications. The TO-loaded NCs were detached from the aqueous suspension by ultracentrifugation at 45,000 rpm at 4 °C for 1 hour and lyophilized at -85 °C for 24 hours. The mass of dried NCs was recorded, while the amount of TO in the supernatant was quantified using UHPLC. Briefly, the sample was diluted with ethanol and filtered by a 0.45 µm syringe filter before injection into the column at 33 °C. The mobile phase used was a mixture of water and acetonitrile (25:75) with isocratic elution. The injection volume was 20 µL with a 0.5 mL/min flow rate. A diode array detector was used to detect the sample at a wavelength of 254 nm. The chromatographic analysis data running time was 30 min per sample with standard *ar*-turmerone eluted at a retention time of 12.8 min. The quantity of turmeric oil in the NCs was computed as the difference between the total amount of turmeric oil initially added into the formulation (Turmeric oil formulation) and the amount of turmeric oil present in the supernatant (Turmeric oil supernatant). The percentage of encapsulation efficiency (% EE) and loading capacity (% LC) were evaluated using Eq. 3 and 4, respectively:

$$EE = \frac{(TO_{\text{formulation}} - TO_{\text{supernatant}})}{TO_{\text{formulation}}} \times 100 \quad (3)$$

$$LC = \frac{(TO_{\text{formulation}} - TO_{\text{supernatant}})}{\text{Dry mass of NCs}} \times 100 \quad (4)$$

*In-vitro* release study of TO from FA-CS/Alg NCs and TO-CS/Alg NCs was performed using a dialysis membrane diffusion method based on the procedure reported by Rajkumar V., et al. (111) with slight modifications. The dialysis bag was first soaked in the medium for 24 h before the start of the experiment (112). Phosphate-buffered saline (PBS) solution (1 mg/mL potassium dihydrogen phosphate, 2 mg/mL dipotassium hydrogen phosphate, 8.5 mg/mL sodium chloride in deionized water, pH 7.4) and acetate-buffered solution (50 mg/mL sodium acetate in 1% acetic acid, adjust the pH with 4.2 g/L sodium hydroxide to pH 5.5) were prepared to mimic the blood and tumor microenvironment, respectively. To maintain sink conditions, 40% (v/v) ethanol was added to the medium. TO-FA-CS/Alg and TO-CS/Alg suspensions (20 mL) were added into the dialysis bag and sealed with clips on both ends. The dialysis bag was immersed in the releasing medium (500 mL) and maintained at 37 °C under continuous gentle agitation. Sampling times were set within 0 to 24 h, wherein 5 mL of medium were withdrawn at specific time points. The withdrawn samples were replaced with an equal volume of fresh medium to maintain sink condition (113). The concentration of TO in the medium was quantified using UHPLC and calculated against the calibration curve. The cumulative percentage of released TO was calculated using Eq. (5):

$$\text{Cumulative release [\%]} = \frac{\text{Turmeric oil release}}{\text{Turmeric oil formulation}} \times 100 \quad (5)$$

The data were fitted into various release kinetic models, i.e., zero-order, first-

order, Korsmeyer-Peppas and Hixson-Crowell, using the DDSolver software, Microsoft Excel plugin program (Version 2010, Microsoft Corporation, Redmond, WA). The best-fit model was chosen based on the highest  $R^2$  adjusted and MSC values and the lowest AIC (114).

### **3.2.6. Cell culture**

Human breast cancer cells (MCF-7 and MDA-MB-231) were cultured in Dulbecco's modified Eagle's medium (DMEM) supplemented with 10% fetal bovine serum and 100 units/mL penicillin/streptomycin in a humidified atmosphere of 5%  $\text{CO}_2$  at 37 °C.

### **3.2.7. Determination of cell surface folate receptor expression**

To determine the expression of folate receptor on the cell surface, each cell line was seeded at a density of  $10 \times 10^4$  cells per 500  $\mu\text{L}$  into each well of 24-well culture plates. Cells were incubated 24 h in a humidified atmosphere of 5%  $\text{CO}_2$  at 37°C. Cells were washed with PBS and detached from the plate by adding 2.9 mM EDTA in PBS and incubated at room temperature for 8 min. EDTA solution was removed by centrifugation of cell suspension at 1,800 rpm for 5 min at 4°C. Cells were washed twice with PBS and blocked with 0.5% BSA in PBS. Cells were stained with R-phycoerythrin-conjugated anti-human Folate Receptors by incubating at 4°C in the dark for 30 min. Mouse IgG control antibody was used as an isotype control. Cells were washed twice with PBS. Stained cells were acquired on a BD Accuri C6 (BD Biosciences, USA) flow cytometer, and data were analyzed using FlowJo™ v10.8 Software (BD Life Sciences).

### 3.2.8. Cytotoxicity assay

To determine the cytotoxicity against MCF-7 and MDA-MB-231 cell lines, the cells were seeded and incubated for 24 h at a density of  $3 \times 10^4$  cells per 100  $\mu\text{L}$  into each well of 96-well culture plates. After that, the cells were treated with 5 serial concentrations of pure TO, TO-CS/Alg NC, and TO-FA-CS/Alg NC in a serum-free media and incubated at 37 °C for 24 h. The controls included NCs without TO. After 24-h treatment, the culture media was removed. Then, 100  $\mu\text{L}$  of an MTT reagent (0.5 mg/mL in serum-free media) was added to each well and further incubated at 37°C. After 4 h, the MTT media was removed, and the insoluble formazan crystals were dissolved by adding dimethyl sulfoxide (DMSO). After completely dissolved, the absorbance was measured at 570 nm using a microplate reader (Anthros, Durham, NC). The percentage of cell viability was calculated using Eq. (6):

$$\text{Cell viability [\%]} = \frac{\text{OD Sample}}{\text{OD control}} \times 100 \quad (6)$$

### 3.2.9. Statistical analysis

Three independent replicates were utilized in all experiments and the collected data were expressed as mean  $\pm$  standard deviation. The polynomial equations were generated using multiple linear regression followed by model-fitting with one-way ANOVA using the Design-Expert<sup>®</sup> software 13.0.5.0 (Stat-Ease, Inc., Minneapolis, MN, USA). The cell viability results were analyzed using two-way ANOVA with Tukey HSD as the post hoc test. The  $\text{IC}_{50}$  values for the unencapsulated TO and TO-FA-CS/Alg NCs were determined through a non-linear regression curve fit analysis. All statistical parameters of the cellular assays were generated using GraphPad<sup>®</sup> Prism software 9.3.0 (San Diego, CA, USA). P-values  $<0.05$  were considered statistically significant.

## CHAPTER 4: RESULTS AND DISCUSSION

### 4.1. Synthesis and characterization of FA-CS

The conjugation of FA and CS involved the DCC/NHS reaction (Fig. 9). Even though FA has two carboxyl groups ( $\alpha$  and  $\gamma$ ),  $\gamma$ -COOH of FA is more prone to this reaction due to its stronger electrophilic and less steric properties (120). The carboxylic group was activated with DCC and NHS to form the folic acid NHS ester and its by-product DCU. The final product, FA-CS conjugate, was obtained by forming an amide bond between the activated carbon of FA-NHS ester and the primary amino group of CS. The yield of the FA-CS was 12%.

The degree of grafting of FA into amino groups in final hydrophobic modified CS was determined by UV-Vis spectrophotometer at 363 nm. Previous studies suggested the use of FA powder diluted in alkaline media to a series of gradient FA standard solutions to calculate the amount of FA in FA-CS (47, 115). The FA-CS samples were dissolved in acidic pH considering the solubility of CS in an acidic environment (47, 115). This can be explained by the incorporation of targeting ligand with CS, hence the change in the physicochemical properties of the polymer. It can be noted that the attempt of dissolving FA-CS in an acidic medium can cause the hydrolysis of FA. However, several studies have shown no hydrolysis that had occurred in the pH used that may interfere with the analysis (47, 115).

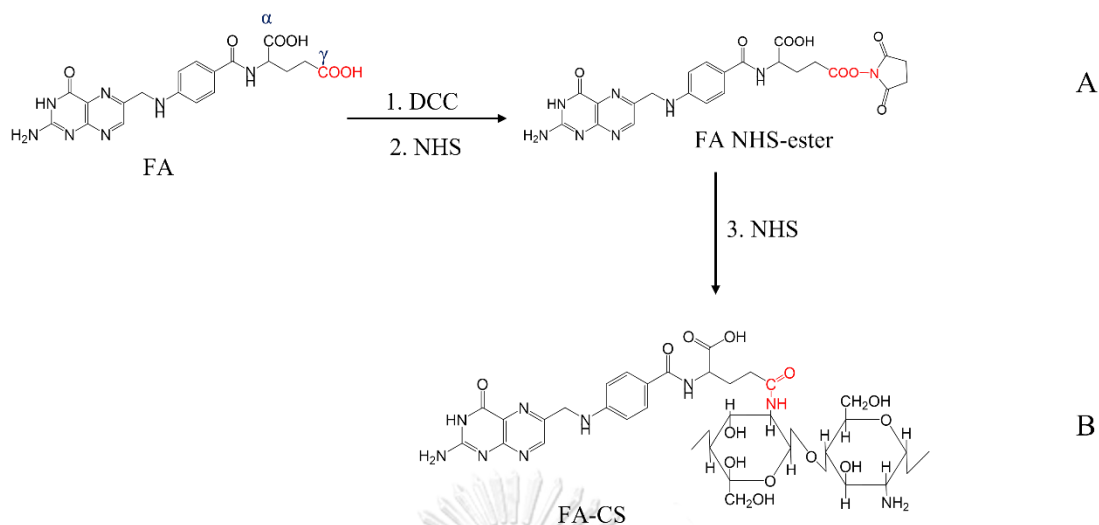


**Figure 9.** Scheme for the synthesis of (A) FA NHS-ester using DCC and NHS in DMSO, 24 h, room temperature; (B) FA-CS using the FA-NHS ester and chitosan solution, 24 h, room temperature

The conjugation between CS and FA to yield FA-CS was confirmed by FT-IR (Fig. 10). The spectra in FA exhibited the bond vibration of C=O and the C=C (aromatic) stretching at  $1688\text{ cm}^{-1}$  and  $1603\text{ cm}^{-1}$ , respectively. The band at  $1482\text{ cm}^{-1}$  represented the stretching C=C and at  $838\text{ cm}^{-1}$  is a characteristic band of the para-substituted benzene ring (47, 116). Moreover, CS spectrum ascribed the O-H and N-H stretching vibration of -OH and -NH<sub>2</sub> functional group at  $3356\text{ cm}^{-1}$  while at  $1639\text{ cm}^{-1}$  and  $1587\text{ cm}^{-1}$  represented to C=O stretching and N-H bending mode amide (N-acetylated CS) and 1° amine, C-O stretching at  $1078\text{ cm}^{-1}$  and peak at  $659\text{ cm}^{-1}$  for the reflecting the pyranoside ring stretching vibration (47, 117). After FA was conjugated with CS, priority bands related to the functional groups of FA and CS suggested the successful conjugation between folic acid and chitosan. Comparing the CS spectrum, the bands at  $1587\text{ cm}^{-1}$  and  $1639\text{ cm}^{-1}$  shift to  $1601\text{ cm}^{-1}$  and  $1650\text{ cm}^{-1}$ , which was assigned to aromatic C=C from the conjugated FA and -C=O of the amide bond and N-H bending of the 2° amine in each in FA-CS spectra.

The  $1650\text{ cm}^{-1}$  peak had a higher transmission than the  $1601\text{ cm}^{-1}$  peak in the FA-CS. These results correspond to a less amide formation, which was consistent with the percentage grafting of FA-CS (12%). The FT-IR results indicate that folic acid's  $\text{-COOH}$  group was successfully conjugated with the  $\text{-NH}_2$  group of chitosan. Furthermore, a band at  $3292\text{ cm}^{-1}$  became broader due to an enhanced hydrogen bonding between FA and CS (116, 117).

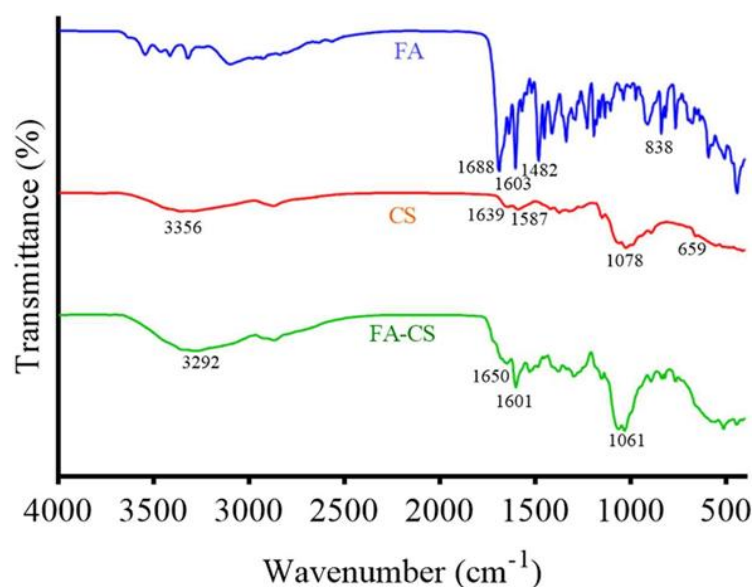


**Figure 10.** FT-IR spectra of FA, CS, and FA-CS

The conjugation of FA and CS was structurally confirmed using  $^1\text{H-NMR}$  (Fig. 11 and Table 9). The signals at 2.50 and 3.30 ppm belong to the DMSO- $d_6$  and water, respectively. Based on the FA spectrum, the characteristic peak at 12.5 and 11.6 ppm was attributed to the  $\text{-COOH}$  proton in the carboxylic group of FA.

However, in the spectrum of FA-CS spectrum, the signal between 3.2-3.9 ppm belongs to the carbon protons of the glucosamine ring of the chitosan. Some of the signals were overlaid by the influence of the solvents and the interactions between the two reactants. Moreover, the FA was successfully conjugated with CS by inspecting

the signal of the FA spectrum at 11.5 ppm shifted to 10.5 ppm in the FA-CS spectrum.

The peak at 7.25 ppm (-NH of amide bond) was newly formed.

**Table 9.** Assignment of  $^1\text{H-NMR}$  spectral data of FA-CS conjugate in  $\text{d}_6\text{-DMSO}$

Position	Chemical shift (ppm)
-COOH	10.5
-NH- (c)	8.6
-NH <sub>2</sub> (e)	6.6
Glucosamine ring of the chitosan	3.2-3.9

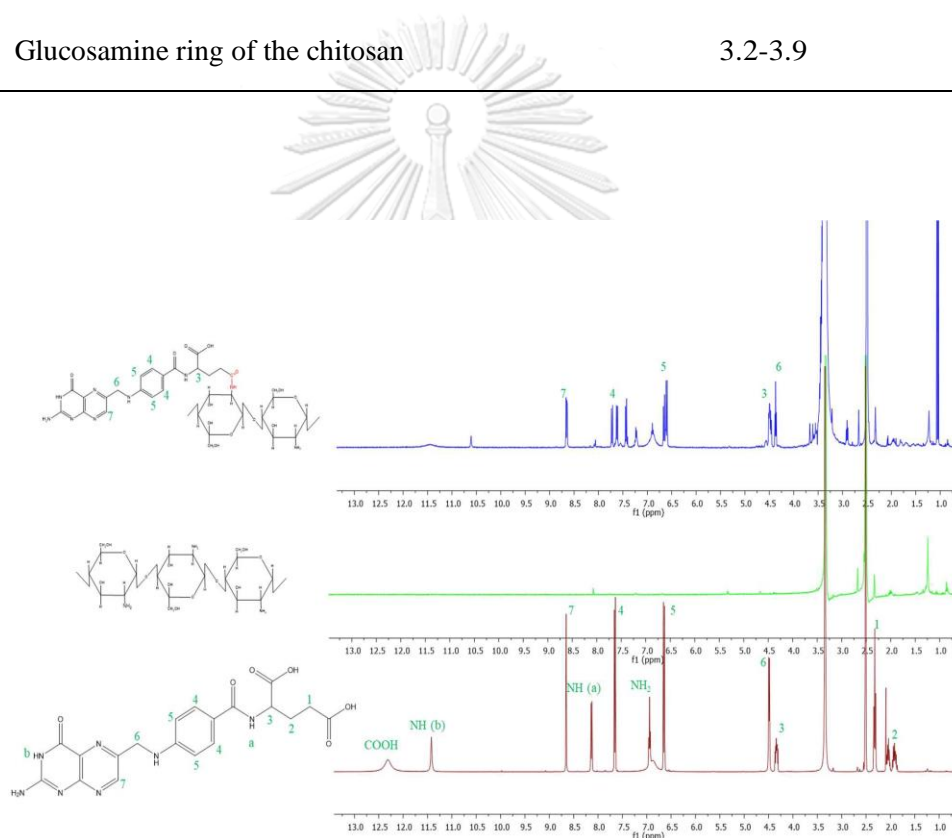


**Figure 11.**  $^1\text{H-NMR}$  spectra of FA-CS, CS, and FA in  $\text{d}_6\text{-DMSO}$

#### 4.2. Assay of *ar*-turmerone content

The main constituents of turmeric oil are bisabolene sesquiterpenes consisting of aromatic turmerone, curlone,  $\alpha$ -turmerone,  $\beta$ -turmerone and bisacumol. Mehrotra N., et al. (118) revealed that *ar*-turmerone (AT) and  $\alpha$ / $\beta$ -turmerone (TU) were analyzed in LC-UV at 240 nm wavelength. The results showed that AT and TU eluted at 9 and



11.5 min, respectively. The calibration curve of *ar*-turmerone was performed by analyzing the standard *ar*-turmerone serial diluted in absolute ethanol concentration in the range of (1-25  $\mu\text{g/mL}$ ) at the wavelength of 254 nm with linear equation ( $y=86.082x+10.617$ ,  $R^2=0.9999$ ) (See Appendix 2). Furthermore, commercial turmeric oil was quantified by using this equation. Commercial turmeric oil contains 12.32 % of *ar*-turmerone. The EE of the nanoformulation was also computed based on that equation.

#### **4.3. Model development for particle size, EE, and LC**

The 3 factors (FA-CS/Alg mass ratio, TO concentration, and poloxamer concentration) were chosen because they primarily affect particle size, EE, and LC based on the literature and preliminary experiments.

Various ratios of the FA-CS and Alg were investigated during the preliminary experiments to determine the maximum working formulation ratio. It was found that the mass ratio 0.07:1 resulted in a dispersion that appeared translucent and no precipitation after 24 h of standing, indicating its stability. Increasing the amount of FA-CS resulted in a gel that was visible in the suspension. Previously, it was demonstrated that increasing the quantities of CS or Alg increased the particle size and the polydispersity index of the NPs and decreased the stability due to the increased viscosity of the dispersion and the presence of an excess amount of polymer by forming clusters of particles (119). Loquercio A., et al. (119) has shown that increasing the polymer ratio could render a more permeable and porous coating, resulting in a reduced entrapment of the hydrophobic compound and subsequent lowering of EE. Decorating the polymeric NP's surface with folate and encapsulating a hydrophobic compound has also shown a higher EE than the plain polymeric NP

(120). Based on the preliminary experiments, increasing the FA-CS/Alg mass ratio resulted in an increase in the yield of the freeze-dried NCs and a consequent decrease in the LC.

It was shown in the literature that increasing the concentration of cinnamaldehyde, a hydrophobic compound, into a polymeric material such as Alg could gradually increase the particle size but an excessive amount of which resulted in a saturation of the wall material, thus causing a decline in the EE and LC. Finding the optimum condition for the TO concentration was therefore important. Based on the preliminary experiments, TO concentration greater than 2 % resulted in a turbid dispersion.

The concentration of poloxamer was also considered in the design of the experiment. The preliminary investigations have shown that the maximum working concentration of poloxamer was 3%. Based on similar studies, an increase in the surfactant concentration led to an increase in the entrapment of the hydrophobic compound, thus increasing the core volume and the particle size. However, a further increase in its concentration resulted in viscous dispersion and partitioning effects causing a decrease in EE and LC (114).

Particle size was a critical response in determining the applicability of the optimized NCs for IV administration. Nanoformulations with sizes below 200 nm would have an efficient passive tumor targeting through the enhanced permeation and retention effect and serve as the first of a series of steps in the cellular uptake of the NPs (121). EE and LC would determine the level of TO in the nanoformulation. The BBD would determine the optimum TO concentration to ensure a successful biological activity.

The advantage of using BBD-RSM is its ability to perform multifactorial analysis on each response with fewer experimental conditions (122). The experimental ranges of the factors were determined through literature review and preliminary experiments. The observed responses for the optimization of the TO-FA-CS/Alg NCs are shown in Table 10. Based on the observed responses, the size of the TO-FA-CS/Alg NCs ranged from 175 to 365 nm, EE between 16.9 to 38.3 %, and an LC ranging from 0.81 to 5.53 %.

**Table 10.** BBD to optimize the TO-FA-CS/Alg NC formulation.

Run	Factors			Responses		
	X <sub>1</sub>	X <sub>2</sub>	X <sub>3</sub>	Y <sub>1</sub>	Y <sub>2</sub>	Y <sub>3</sub>
1	0.03	1.0	1.75	175 ± 21	33.1 ± 1.2	0.88 ± 0.01
2	0.05	1.5	1.75	248 ± 16	28.8 ± 1.4	1.4 ± 0.32
3	0.05	1.0	3.00	250 ± 14	28.0 ± 0.7	0.69 ± 0.12
4	0.05	2.0	3.00	310 ± 18	16.9 ± 1.4	1.11 ± 0.51
5	0.05	1.5	1.75	244 ± 19	28.2 ± 1.8	1.53 ± 0.39
6	0.05	2.0	0.50	365 ± 19	38.3 ± 7.0	5.53 ± 0.20
7	0.07	1.0	1.75	188 ± 8	28.6 ± 1.0	1.04 ± 0.05
8	0.03	2.0	1.75	279 ± 12	29.2 ± 3.0	2.96 ± 0.36
9	0.05	1.0	0.50	230 ± 11	33.2 ± 2.2	2.18 ± 0.08
10	0.03	1.5	3.00	297 ± 9	23.3 ± 0.8	0.81 ± 0.14
11	0.03	1.5	0.50	310 ± 12	37.1 ± 4.2	4.17 ± 0.50
12	0.07	2.0	1.75	279 ± 16	25.6 ± 1.7	2.06 ± 0.31
13	0.05	1.5	1.75	258 ± 19	28.0 ± 1.4	1.47 ± 0.11
14	0.07	1.5	0.50	345 ± 8	33.3 ± 3.4	3.36 ± 0.37
15	0.07	1.5	3.00	278 ± 9	23.0 ± 1.1	0.95 ± 0.18

X<sub>1</sub>: FA-CS/Alg mass ratio; X<sub>2</sub>: TO (% w/v); X<sub>3</sub>: poloxamer 407 (% w/v); Y<sub>1</sub>: particle size (nm); Y<sub>2</sub>: EE (%); Y<sub>3</sub>: LC (%).

The polynomial equations were generated using multiple linear regression to determine the relationship among the factors and the responses. Various statistical parameters were utilized to determine the equations that fit the data well, such as the overall model's significance, lack-of-fit, the significance of each regression coefficient; adjusted  $R^2$ ; and adequate precision based on the ANOVA. Based on the p-value of each regression coefficient, the model reduction was performed by retaining only the significant terms, thus refining and increasing the precision of the models. The results of the regression analyses are presented in Table 11. The overall models show that the coefficients were statistically significant jointly ( $p < 0.0001$ ), indicating that the factors in each model improved its fit. The lack-of-fit test for each model suggests an insignificant lack-of-fit of the regression model ( $p > 0.05$ ), showing that a linear relationship exists between the factor and response. There was also a reasonable agreement between the adjusted  $R^2$  and predicted  $R^2$ , having a difference of less than 2. The adequate precision of the models, measuring the signal-to-noise ratio, were all greater than 4, indicating that the design space can be navigated with precision.

**Table 11.** Summary of the regression analyses of the responses

Response	Suggested model	p-value, overall model	p-value, lack-of-fit	Adj $R^2$	Pred $R^2$	Adeq precision
Particle size	Quadratic	< 0.0001	0.5347	0.9787	0.9220	34.6723
EE	2FI	< 0.0001	0.2620	0.9820	0.9635	44.0165
LC	Quadratic	< 0.0001	0.1039	0.9859	0.9641	38.5856

The well-fitted particle size and LC was EE, and LC models were quadratic, 2-factor interaction, and linear models, respectively (Equations 7–9). The 3D surface

plots for  $Y_1$  to  $Y_3$  show the interactive effects of two factors while the other factor can be navigated within the design space (Fig. 12).

$$Y_1 = 249.79 + 3.60X_1 + 48.68X_2 - 14.38X_3 - 13.65X_1X_3 - 18.62X_2X_3 - 19.32X_2^2 + 57.99X_3^2 \quad (7)$$

$$Y_2 = 28.96 - 1.56X_1 - 1.62X_2 - 6.32X_3 + 0.9025X_1X_3 - 4.05X_2X_3 \quad (8)$$

$$Y_3 = 1.62 - 0.1762X_1 + 0.8587X_2 - 1.46X_3 - 0.2650X_1X_2 + 0.2375X_1X_3 - 0.7325X_2X_3 + 0.7300X_3^2 \quad (9)$$

The positive regression coefficients in the RSM models indicate a direct relationship between a factor and a response. In contrast, negative values indicate an inverse relationship between a factor and the observed response.

Equation (7) shows that as  $X_1$  and  $X_2$  increased, the size of the TO-FA-CS/Alg NCs also increased, with  $X_2$  having the most significant effect, as shown in Fig 12 (b) and (c). These observed effects were due to an increase in the viscosity of the dispersion and the additional surface coating layers of the grafted chitosan as its concentration was increased in the dispersion (123). Another study showed that the grafting of folate with chitosan resulted in slightly larger nanocapsules than the chitosan-coated nanoparticles alone (124). Further increasing the concentration of  $X_2$  would remarkably increase the size of the nanoparticles. The size of the TO-FA-CS/Alg NCs increases by a factor of 48.7 nm with every 1% increase in  $X_2$ . This effect could be due to the amphiphilic nature of poloxamer 407 and the consequent increase in the size of the micelle core of the NCs with additional quantities of TO being added into the formulation. Fig 12 (a) and (b) show that an increase of  $X_3$  from a low to intermediate concentration decreased the size of the nanoparticles. A lower concentration of the surfactant was not sufficient to encapsulate the hydrophobic TO. Increasing  $X_3$  could have caused the formation of a stronger barrier of the micelle core by achieving the

minimum size near the minimum level of  $X_3$  but within the experimental range. Further, an increase of  $X_3$  resulted in a remarkable increase in the size, probably due to the increased viscosity and near saturation of the aqueous phase with the micelle cores, consequently resulting in aggregation (125). The excess amount of poloxamer 407 in the dispersion could have interacted with the outer grafted chitosan layer resulting in a bigger nanocapsule size.

The EE of TO-FA-CS/Alg NCs was most significantly affected by  $X_3$  and almost similar  $X_1$  and  $X_2$  as shown in Equation (5) and Fig 12 (d-f). The reduced capacity of the NCs to encapsulate TO was mainly due to the effect of  $X_3$  (poloxamer concentration). In the formulation of the NCs, TO was added into a mixture of poloxamer 407 and alginate matrix. The miscibility of TO with the aqueous phases increased with the addition of poloxamer 407. Further increasing  $X_3$  resulted in a saturation of the aqueous dispersion with micelles until the critical micelle concentration was achieved (126). At this point, increasing  $X_3$  would have a negligible impact on the encapsulation of TO. In another study, further increasing the concentration of Pluronic F-127 resulted in an insignificant increase in EE (124). Due to the dispersion viscosity, these effects can be attributed to the hindered encapsulation of TO within the hydrophobic micelle core. The main effects of  $X_1$  and  $X_2$  were then considered second only to the impact of  $X_3$ , where the grafted chitosan served to decrease the permeability and consequently the leakage of TO from the core of the NCs by electrostatically interacting with the alginate matrix (11).

The LC of TO-FA-CS/Alg NCs was directly affected by  $X_2$ , indicating that LC increased with  $X_2$  (Fig 12 h and i). The negative regression coefficients of  $X_1$  and  $X_3$

show their inverse effects on LC, with the most significant impact on LC demonstrated by  $X_3$  (Fig 12 g and h). The increasing levels of  $X_1$  and  $X_3$  resulted in a lower LC because of the additional mass of the nanoparticles conferred upon by the grafted polymer and surfactant, respectively. The latter figures also show the curvilinear effects of  $X_3$ , with the maximum LC being achieved within minimum levels of  $X_3$  based on the design space. The LC was observed to increase with an increase in  $X_2$  due to the higher capacity of the surfactant-polymer system to accommodate additional amounts of TO but only until a certain point, as shown in Fig 12 (g).

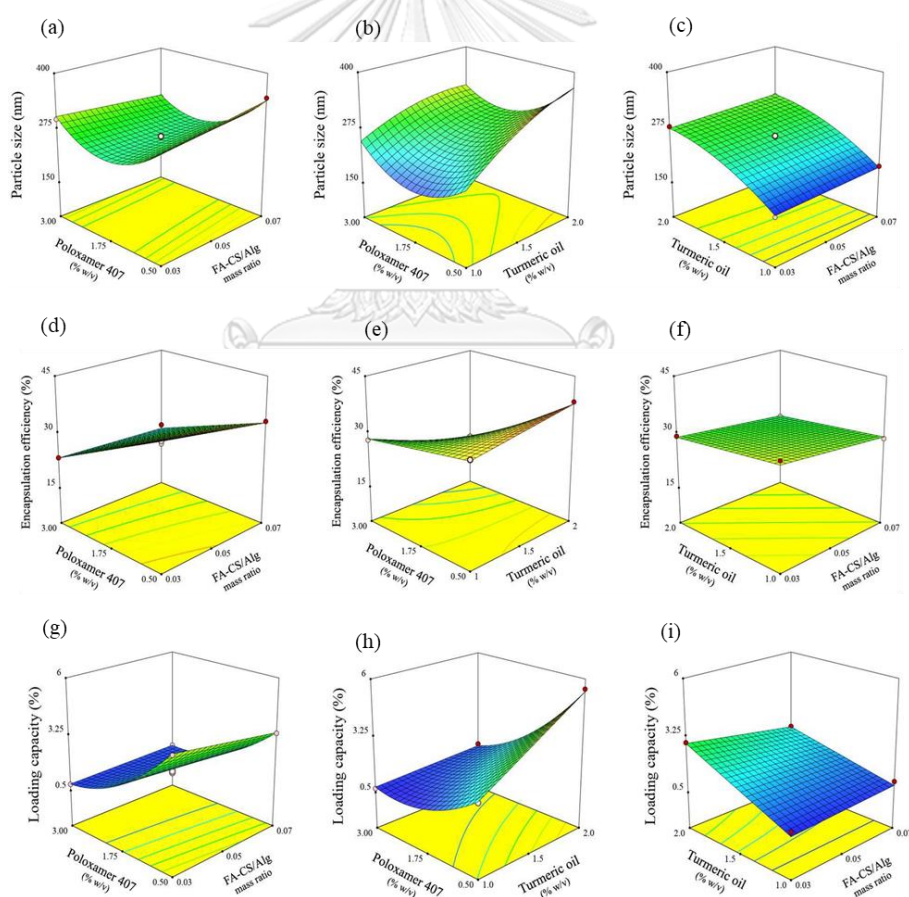


**Figure 12.** Response surface plots showing the effects of FA-CS/Alg mass ratio ( $X_1$ ), turmeric oil concentration ( $X_2$ ), and poloxamer 407 concentration ( $X_3$ ) on (a-c) particle size ( $Y_1$ ), (d-f) EE ( $Y_2$ ), and (g-i) LC ( $Y_3$ ).

#### 4.4. Validation of the response surface model

To validate the generated RSM models, the TO-FA-CS/Alg NCs were formulated based on the optimum conditions of the FA-CS/Alg mass ratio (0.03), TO concentration (1.0 %), and poloxamer 407 concentration (0.65 %) at desirability (D) of 0.961, which was closer to 1.0. Of particular interest is the optimum concentration for poloxamer, which was found to be 0.65%. This concentration was at the lower end of the 0.5 to 3.0 % working range in the optimization experiments. Using this concentration, the particle size was between 175 and 365 nm, which would be acceptable for IV administration. The EE and LC were between 16.9-38.3% and 0.81-5.53%, respectively. Considering the biological applications of the optimized nanocapsules, an increase in the concentration of Poloxamer would increase its toxicity in normal cells both *in vitro* and *in vivo* (19). Therefore, a minimum poloxamer concentration (0.65 %) provided acceptable outcomes for this study. TO-CS/Alg NCs were fabricated under the same conditions CS/Alg mass ratio (0.03), TO concentration (1.0 %), and poloxamer 407 concentration (0.65 %) by ionotropic gelation method to determine the biological assay.

The values of the observed responses were compared with the predicted responses for particle size, EE, and LC. A good agreement between the observed and predicted responses was found with all % error values below 10%, indicating the high predictive ability of the developed RSM models (Table 12).



**Table 12.** Validation of the prediction capability of the RSM models

Optimized condition	Response	Predicted response	Observed response	%Error
X <sub>1</sub> : 0.03 FA-CS/Alg mass ratio	Y <sub>1</sub> (nm)	207	189 ± 4	8.6
X <sub>2</sub> : 1.0% TO	Y <sub>2</sub> (%)	34.9	35.9 ± 13.5	2.7
X <sub>3</sub> : 0.65% Poloxamer 407	Y <sub>3</sub> (%)	2.08	1.82 ± 0.39	0.12

The observed size of the optimized TO-FA-CS/Alg NCs was about 189 nm. The combined effects of the particle size and folate grafting of the outer chitosan chain facilitate a more accessible diffusion of the NCs into the tumor cells and significantly increase cellular internalization. This approximate size could also mean that the formulation can be administered intravascularly without concerns of embolization (127). The observed results for EE and LC were expected as TO is a hydrophobic compound, and this study utilized hydrophilic polymers. Some studies using a polyelectrolyte complex of chitosan and alginate showed similar results for the encapsulation of hydrophobic compounds (128, 129). The results showed an average size of 189±4 nm and PDI of 0.192±0.1, which is close to 0, indicating the highly homogenous distribution among the particles (Fig. 13A) (130). Zeta potential was also determined to predict the stability of NCs in the aqueous system based on its surface charge. The NCs render a negative zeta potential value of about -12.61± 2.3 (Fig. 13B). The zeta potential was significantly decreased after the modification of CS with FA. This might be a partial substitution of -NH<sub>2</sub> of CS with FA (47). The morphology of TO-FA-CS/Alg NCs was visualized by TEM after diluting the nanosuspension 50x in ultrapure water. The NCs were spherical and had smooth surfaces with a particle size of approximately 200 nm (Fig.13C-D). It was evident in the image that a thin layer of FA-

CS was coated onto TO-Alg NCs as indicated by the arrow shown in Fig. 13D.

The physical stability of the TO-CS/Alg NCs was previously demonstrated at 4 °C and 25 °C for 120 days in suspension form (11). However, for the current study, the physical and chemical stabilities of the TO-FA-CS/Alg NCs at 4 °C and 25 °C for 3 months are currently being investigated. The NCs are evaluated in terms of particle size, zeta potential, and encapsulation efficiency.

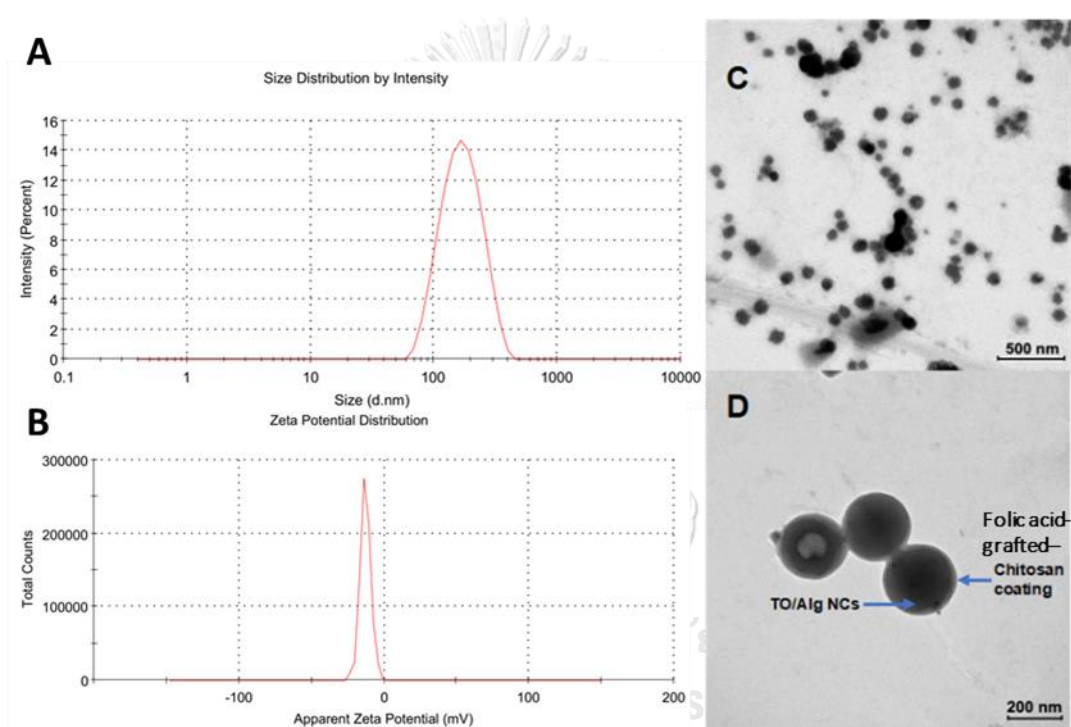


**Figure 13.** Physical characteristics of TO-CS/Alg NCs: (A) Size distribution by intensity, (B) Zeta potential distribution, (C and D) TEM images at 50,000 and 100,000x magnification, respectively.

#### 4.5. *In vitro* release kinetics study

A sustained-release profile, minimal release in the blood circulation, and maximal release in the tumor tissues are the necessary attributes of this nanoformulation. The release of TO from the TO-FA-CS/Alg NCs and TO-CS/Alg NCs in both pH 7.4 and pH 5.5 were studied. As shown in Fig. 14, the unencapsulated TO was spontaneously

released at the first 2 h, and almost 60% of the initially added TO were released after 7 h in both media. Meanwhile, the release of TO from both NCs was slower than the unencapsulated TO in both media. After 12 h, the release of TO from both NCs was estimated to be at 50% and exhibited a sustained release. Furthermore, TO release in low pH media was higher than in neutral or alkaline media. This phenomenon can be explained by the increased solubilization of CS in acidic media, causing the leakage of the encapsulated TO through the porous CS/Alg NCs into the releasing media (123). However, the TO from TO-FA-CS/Alg NCs was a bit more released than from TO-CS/Alg NCs after 3 hours in alkaline media. This was due to the different chemical structures on the backbone of chitosan and the solubility in the different media in terms of the effect of diffusion rate via the inner structure of the system. In contrast, TO from the NCs was slowly released in alkaline media because of CS shrinkage, which prevented the release of encapsulated TO from CS/Alg NCs (123). These results demonstrate that FA-CS/Alg NCs can serve as a sustained and controlled release carrier for oral and intravenous administration of TO (131).

It can also be hypothesized that the FA-CS/Alg could be a potential carrier of TO for oral administration in future studies. For instance, FA-grafted CS has successfully loaded insulin for its oral administration and treatment of diabetes mellitus (132). In this study, the release profiles have shown that the FA-grafted CS released insulin in a sustained manner in simulated gastric fluid (SGF, pH 1.2), simulated intestinal fluid (SIF, pH 6.8) and PBS (pH 7.4). The uptake studies in Caco-2 cell lines showed that the FA-grafted CS demonstrated a higher internalization of insulin than the plain CS-coated NP.

The DDSolver was used to evaluate the release profile of TO from the nanoparticles and determine the model that best describes this release profile. In two media, the in vitro release data of TO from the TO-CTS/Alg NCs and TO-FA-CS/Alg NCs formulations were fitted to Korsmeyer-Peppas. This model showed the highest coefficient of determination ( $R^2$ ), lowest AIC, and maximal MSC values. Additionally, the Korsmeyer-Peppas model showed that the release exponent ( $n$ ) of TO from the TO-FA-CS/Alg NCs in the two media was in the range of 0.345–0.387 (Table 13) and that from the TO-CS/Alg NCs in the two media was in the range of 0.356–0.455 (Table 14). These data indicate that the drug release followed the Fickian diffusion-controlled release pattern ( $n < 0.5$ ), which could be inferred as the controlling factor for the diffusion of TO through the pore of FA-CS/Alg NCs based on the TO concentration gradient, that can be used for a controlled and sustained drug release dosage form. Accordingly, these results can be used to further design and develop TO-FA-CS/Alg NCs for the required administration route (133).

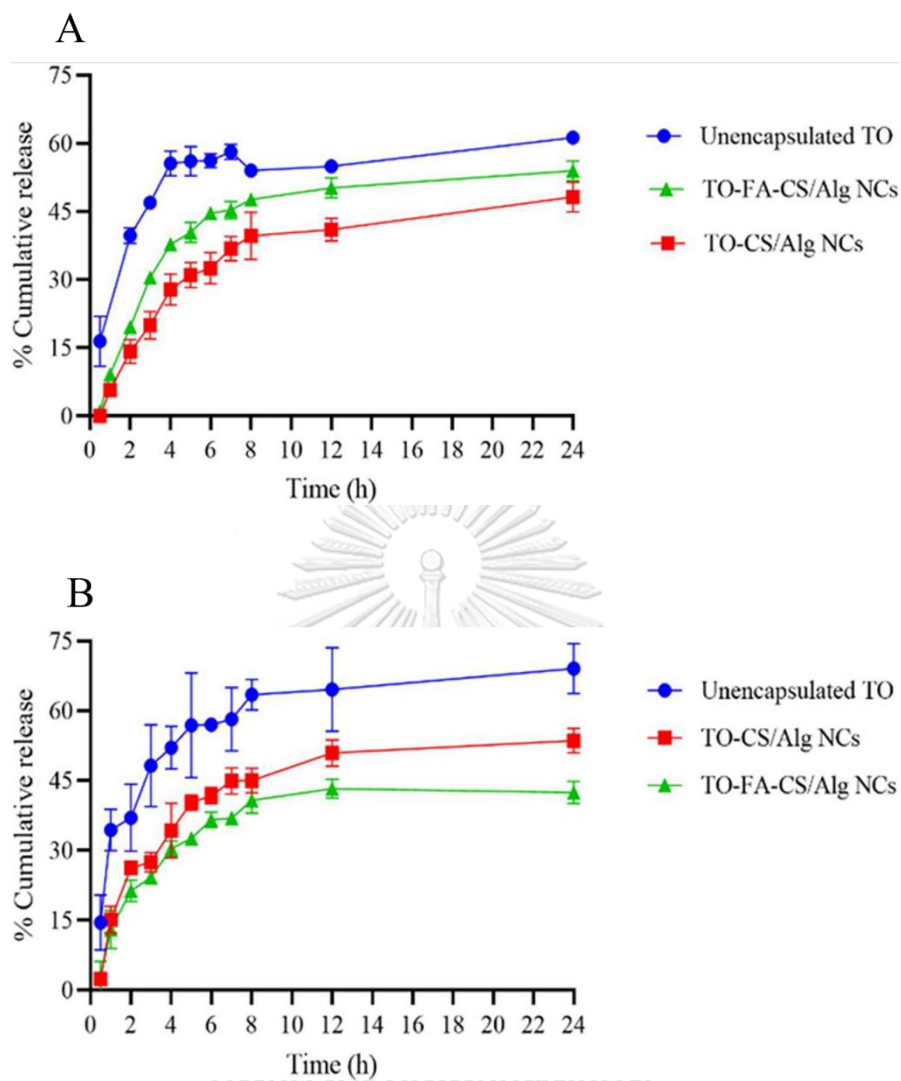


**Figure 14.** Percent cumulative release of TO from the unencapsulated TO, TO-FA-CS/Alg NCs, and TO-CS/Alg NCs in (A) pH 7.4 and (B) pH 5.5.

**Table 13.** Release kinetics of TO from TO-FA-CS/Alg NCs

Model	Media	Parameter	R <sup>2</sup> adjusted	AIC	MSC
Zero order (F = k <sub>0</sub> .t)	pH 5.5	k <sub>0</sub> = 2.976	-0.7961	90.1318	-0.9216
	pH 7.4	k <sub>0</sub> = 3.633	-0.3075	93.3060	-0.4488
First order (F = k <sub>KP</sub> .t <sup>n</sup> )	pH 5.5	k <sub>1</sub> = 0.053	0.0774	82.8555	-0.2601
	pH 7.4	k <sub>1</sub> = 0.075	0.5321	81.9675	0.5820
Higuchi (F = k <sub>H</sub> . t <sup>0.5</sup> )	pH 5.5	k <sub>H</sub> = 12.116	0.6697	71.6241	0.7609
	pH 7.4	k <sub>H</sub> = 14.603	0.7513	75.0397	1.2118
<sup>a</sup> Korsmeyer- Peppas (F = k <sub>H</sub> . t <sup>n</sup> )	pH 5.5	k <sub>KP</sub> = 17.166, n = 0.345	0.7879	67.3280	1.1515
	pH 7.4	k <sub>KP</sub> = 18.819, n = 0.387	0.7863	74.2195	1.2863
Hixson-Crowell (F = 100 · [1 - (1 - k <sub>H</sub> C · t) <sup>3</sup> ])	pH 5.5	k <sub>HC</sub> = 0.015	-0.1687	85.4417	-0.4952
	pH 7.4	k <sub>HC</sub> = 0.021	0.34170	85.7354	0.2394

<sup>a</sup>Best-fit release kinetics model for TO-FA-CS/Alg NCs. F is the fraction (%) of drug released in time, t; k<sub>0</sub> is the zero-order release constant; k<sub>1</sub> is the first-order release constant; k<sub>KP</sub> is the release constant incorporating structural and geometric characteristics of the drug-dosage form; n is the diffusional exponent indicating the drug-release mechanism; k<sub>HC</sub> is the Hixson-Crowell release constant.

**Table 14.** Release kinetics of TO from TO-CS/Alg NCs

Model	Media	Parameter	R <sup>2</sup> adjusted	AIC	MSC
Zero order (F = k <sub>0</sub> .t)	pH 5.5	k <sub>0</sub> = 3.705	-0.5653	92.8533	-0.6268
	pH 7.4	k <sub>0</sub> = 2.813	0.1404	85.73.10	-0.3866
First order (F = k <sub>KP</sub> .t <sup>n</sup> )	pH 5.5	k <sub>1</sub> = 0.078	0.4225	81.9190	0.3672
	pH 7.4	k <sub>1</sub> = 0.0654	0.6207	76.7129	0.4332
<sup>a</sup> Korsmeyer- Peppas (F = k <sub>H</sub> . t <sup>n</sup> )	pH 5.5	k <sub>KP</sub> = 20.650, n = 0.356	0.8352	68.9600	1.5453
	pH 7.4	k <sub>KP</sub> = 11.442, n = 0.455	0.8390	68.2227	1.2050
Hixson-Crowell (F = 100 · [1 - (1 - k <sub>HC</sub> · t) <sup>3</sup> ])	pH 5.5	k <sub>HC</sub> = 0.018	0.1962	85.5535	0.0368
	pH 7.4	k <sub>HC</sub> = 0.013	0.4935	79.9011	0.1433

<sup>a</sup>Best-fit release kinetics model for TO-FA-CS/Alg NCs. F is the fraction (%) of drug released in time, t; k<sub>0</sub> is the zero-order release constant; k<sub>1</sub> is the first-order release constant; k<sub>KP</sub> is the release constant incorporating structural and geometric characteristics of the drug-dosage form; n is the diffusional exponent indicating the drug-release mechanism; k<sub>HC</sub> is the Hixson-Crowell release constant.

#### 4.6. Folate receptor expression level

MBA-MD-231 and MCF-7 are breast cancer cell lines. MBA-MB-231 cell is a kind of TNBC cell that lacks either the expression of estrogen/progesterone or HER 2 receptors. MCF-7 is derived from the epithelium layer of breast cancer cells. Both cell lines express folate receptors on their surfaces. The folate receptor expression levels of MDA-MB-231 was 1.6-fold than that of MCF-7 (Fig. 15).

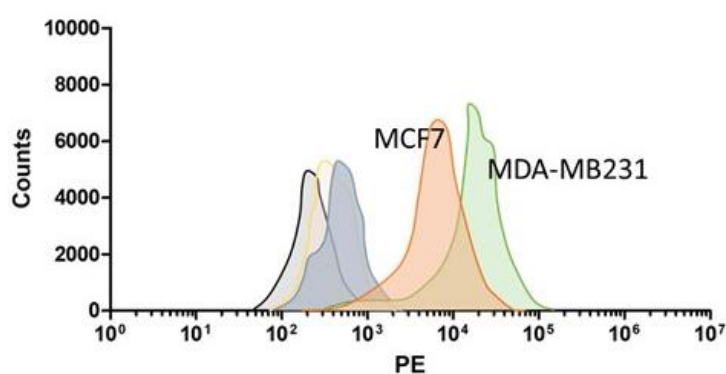


**Figure 15.** Folate expression levels in MDA-MB-231 and MCF-7 cell lines

#### 4.7. Cytotoxicity assay

The toxicities of the unencapsulated TO (positive control), CS/Alg NC and FA-CS/Alg NC (negative controls), TO-CS/Alg NC, and TO-FA-CS/Alg NC (turmeric oil-loaded nanocapsules) were evaluated with TO concentrations ranging from 20 to 100  $\mu\text{g}/\text{mL}$  for 24 h using the MTT assay against MDA-MB-231 and MCF-7 breast cancer cells (Fig. 16).

Using Tukey HSD to compare the treatments, there was a significant difference in the viability of MDA-MB-231 between the control and both TO-CS/Alg NC and TO-FA-CS/Alg NC starting at 80  $\mu\text{g}/\text{mL}$ . However, the significant difference in the viability of MCF-7 between the control and both TO-CS/Alg NC and TO-FA-CS/Alg NC occurred at 80  $\mu\text{g}/\text{mL}$  and 40  $\mu\text{g}/\text{mL}$ , respectively. The viabilities of MDA-MB-



231 and MCF-7 with the treatments for each concentration were also compared. TO-CS/Alg NCs and TO-FA-CS/Alg NCs were more potent than the unencapsulated TO from 80 to 100  $\mu\text{g/mL}$  against both breast cancer cell lines. TO-FA-CS/Alg NC was more toxic than TO-CS/Alg NC toward MDA-MB-231 at 80  $\mu\text{g/mL}$ . However, TO-FA-CS/Alg NC was more toxic than TO-CS/Alg NC toward MCF-7 from 40 to 80  $\mu\text{g/mL}$ . CS/Alg NC and FA-CS/Alg NC (negative control) had a dose-dependent cytotoxic effect. This effect would be due to the poloxamer concentration (135). Free TO in nanosuspension can kill the cells. Even though, in this study, TO-FA-CS/Alg NC decreased the viability of breast cancer cells due to the internalization via the folate receptors expressing on the cell surface.

The  $\text{IC}_{50}$  values of the unencapsulated TO, TO-CS/Alg NCs, and TO-FA-CS/Alg NCs against MDA-MB-231 and MCF-7 are presented in Table 15. The results show that the  $\text{IC}_{50}$  values of TO-CS/Alg NCs and TO-FA-CS/Alg against both cell lines differed significantly from the unencapsulated TO. Further, the  $\text{IC}_{50}$  values of TO-FA-CS/Alg NC on both cell lines were significantly different from TO-CS/Alg NC.

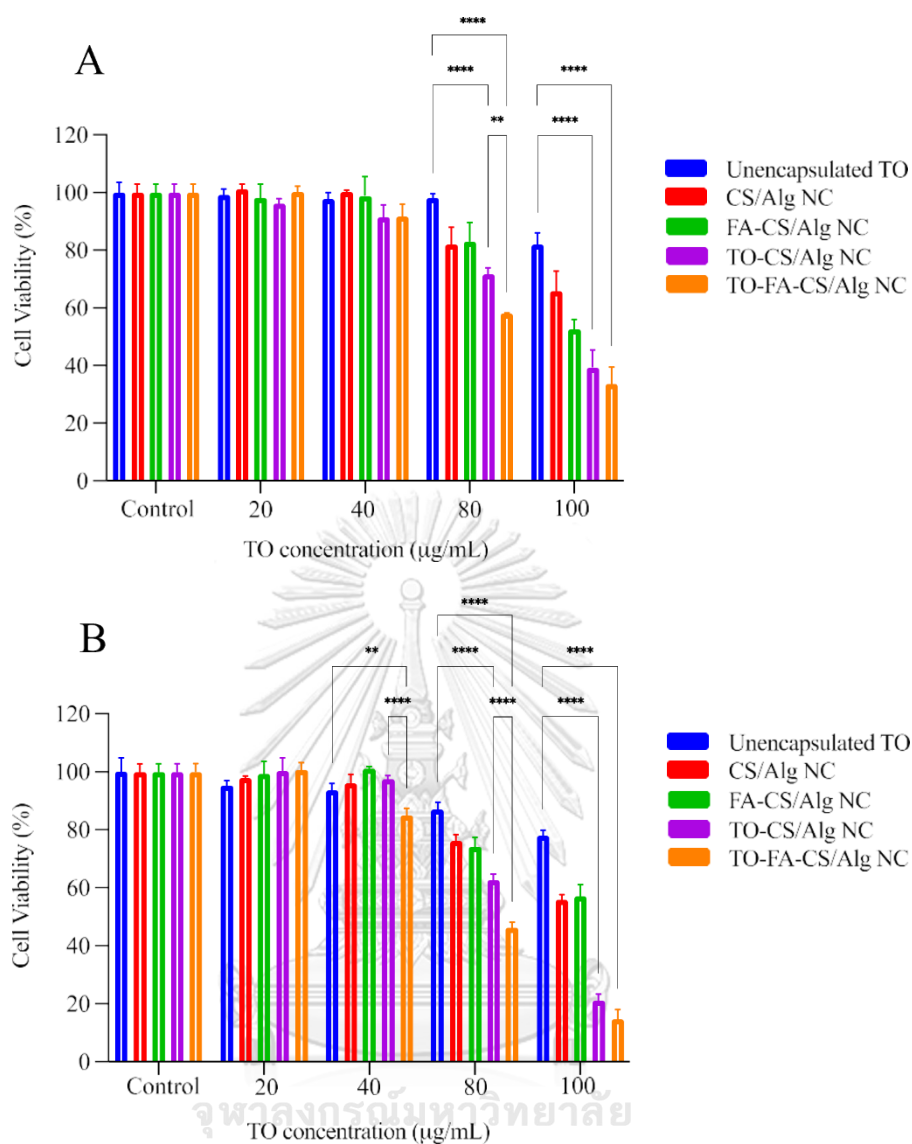


**Figure 16.** The viability of (A) MDA-MB-213 and (B) MCF-7 treated with TO (positive control), CS/Alg NC and FA-CS/Alg NC (negative controls), and TO-CS/Alg NC and TO-FA- CS/Alg NC (turmeric oil-loaded nanocapsules) containing different TO concentrations.

The (\*) represents pairwise comparisons that show statistically significant differences among the treatments within each concentration of TO ( $p < 0.05$ ).

**Table 15.** Mean IC<sub>50</sub> values of the unencapsulated TO, TO-CS/Alg NCs, and TO-FA-CS/Alg NCs against MDA-MB-231 and MCF-7 cell lines

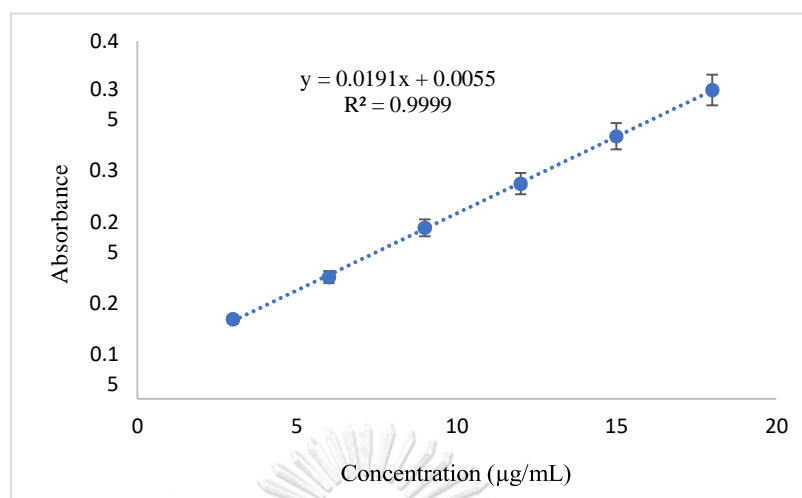
Treatment	IC <sub>50</sub> (µg/mL)	
	MDA-MB-231	MCF-7
Unencapsulated TO	122.8 ± 2.8	139.7 ± 4.0
TO-CS/Alg NC	95.1 ± 6.0*	85.2 ± 1.1*
TO-FA-CS/Alg NC	85.3 ± 2.8* <sup>^</sup>	71.1 ± 1.1* <sup>#</sup>

\*p<0.0001 (compared to unencapsulated TO), <sup>^</sup>p=0.0125 (compared to TO-CS/Alg NC), <sup>#</sup>p=0.0009 (compared to TO-CS/Alg NC)

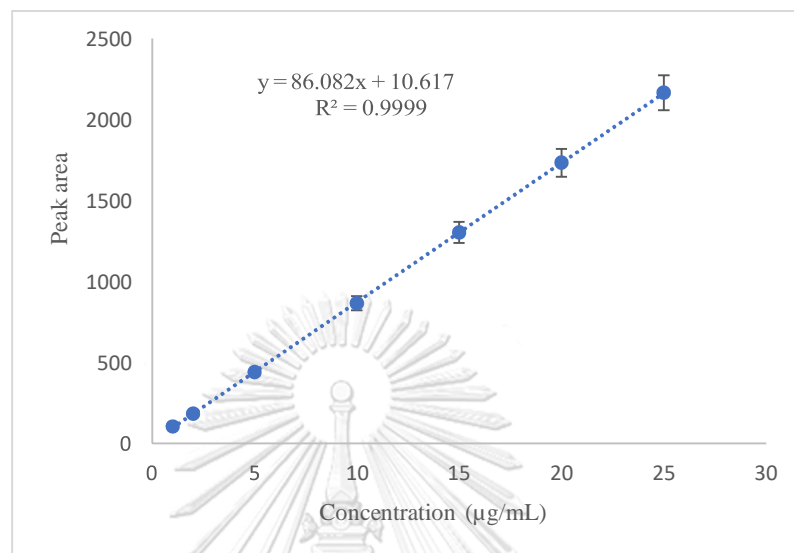
Overall, TO-FA-CS/Alg NC exhibited a significantly higher toxicity level than TO-CS/Alg NC and unencapsulated TO against both breast cancer cells, signifying that FA-CS/Alg NC can enhance the toxicity effects of TO against both invasive MDA-MB-231 and MCF-7 breast cancer cells. The higher cytotoxicity of TO-FA-CS/Alg NCs can be attributed to the interaction of the folic acid-grafted chitosan with the folate receptors that are overexpressed on the membrane of MDA-MB-231 and MCF-7 (56, 92).

## CHAPTER 5: CONCLUSION

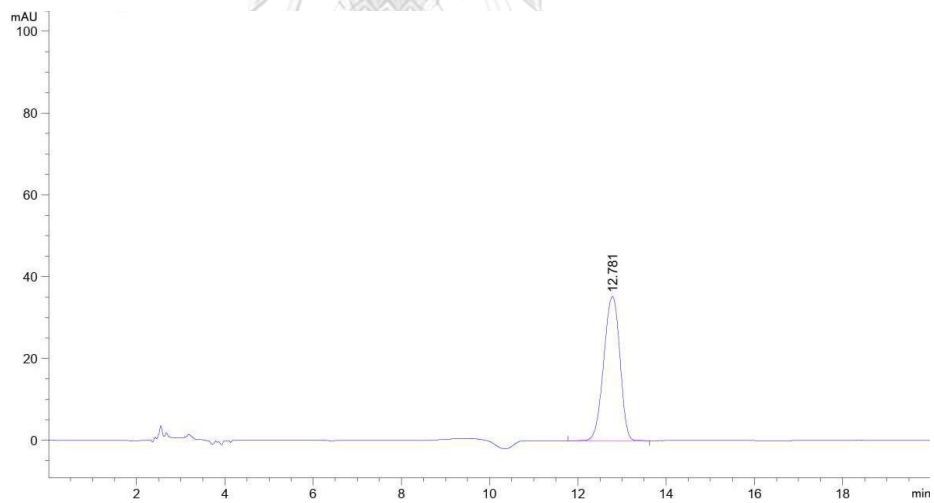
The conjugation of FA with CS involved an amide reaction using NHS/DCC.  $\gamma$ -carboxyl group of folic acid was activated by DCC/NHS to form the FA NHS-ester and by-product DCU which can easily remove by filtration. The activated FA NHS-ester was grafted with a primary amino group of CS to form the amide bond.  $^1\text{H-NMR}$  and FT-IR confirmed the synthesized FA-CS with a degree of substitution of 12% by UV-Vis. TO-FA-CS/Alg NCs were prepared via ionotropic gelation by the electrostatic interaction between the  $-\text{COOH}$  groups of alginates and  $-\text{NH}_2$  of chitosan. The fabrication of TO-FA-CS/Alg NCs was successfully optimized using the BBD rendering good particle size (189 nm) with modest aggregation and high EE (35.9%) and LC (1.82%). Cell viability assay revealed that the TO-FA-CS/Alg NC was more toxic than TO-CS/Alg NC and unencapsulated TO against folate-receptor positive MDA-MB-231 and MCF-7 breast cancer cell lines. In prospect, the TO-FA-CS/Alg NCs can be further evaluated in a preclinical study for breast cancer therapy.

**Appendix 1.** Calibration curve of FA by measuring the absorbance at 363 nm

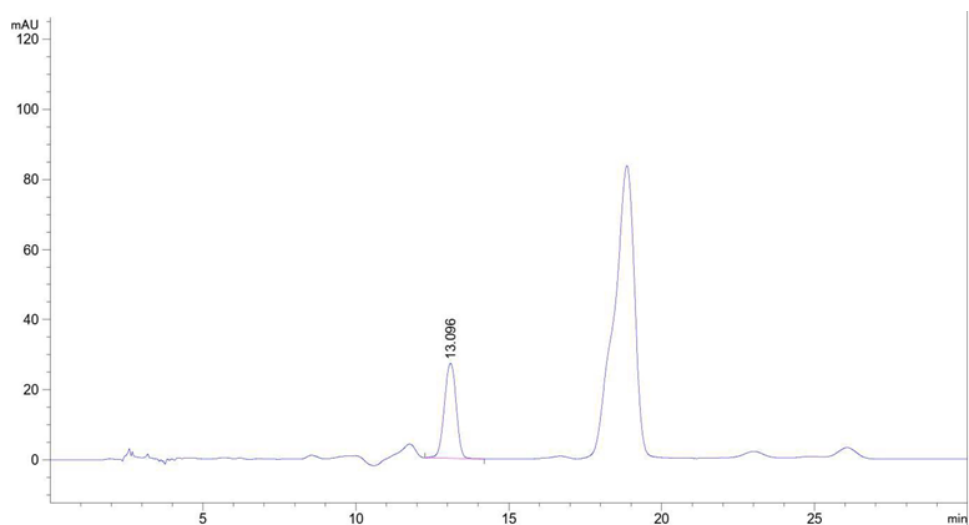
**Appendix 2.** (A) Calibration curve of *ar*-turmerone, UHPLC condition of (B) *ar*- turmerone and (C) turmeric oil



(A)



(B)

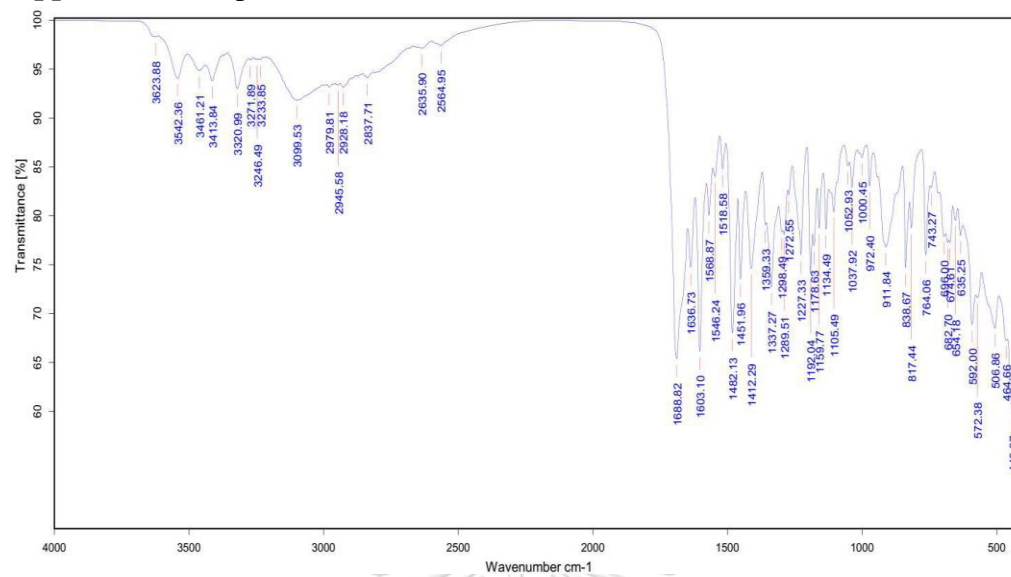


(C)

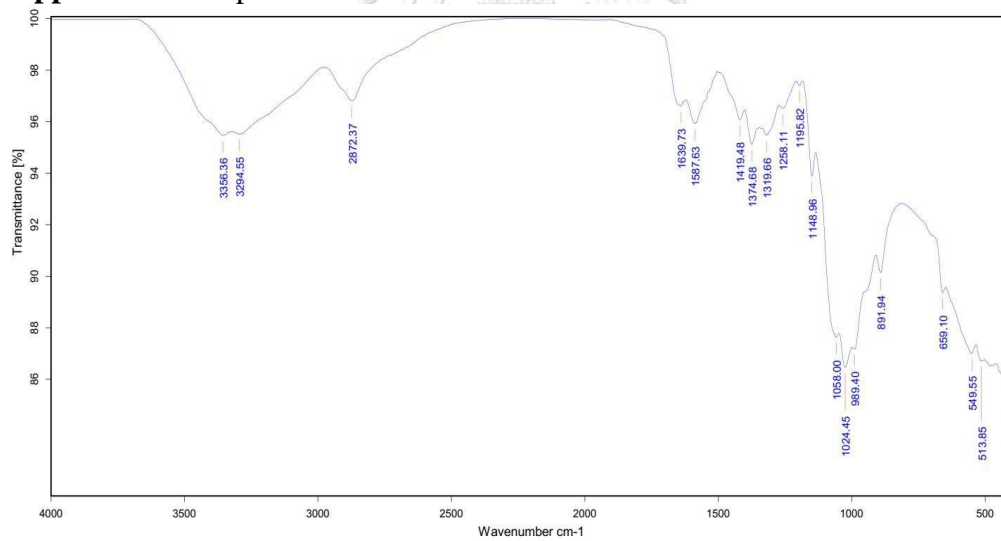


จุฬาลงกรณ์มหาวิทยาลัย  
CHULALONGKORN UNIVERSITY

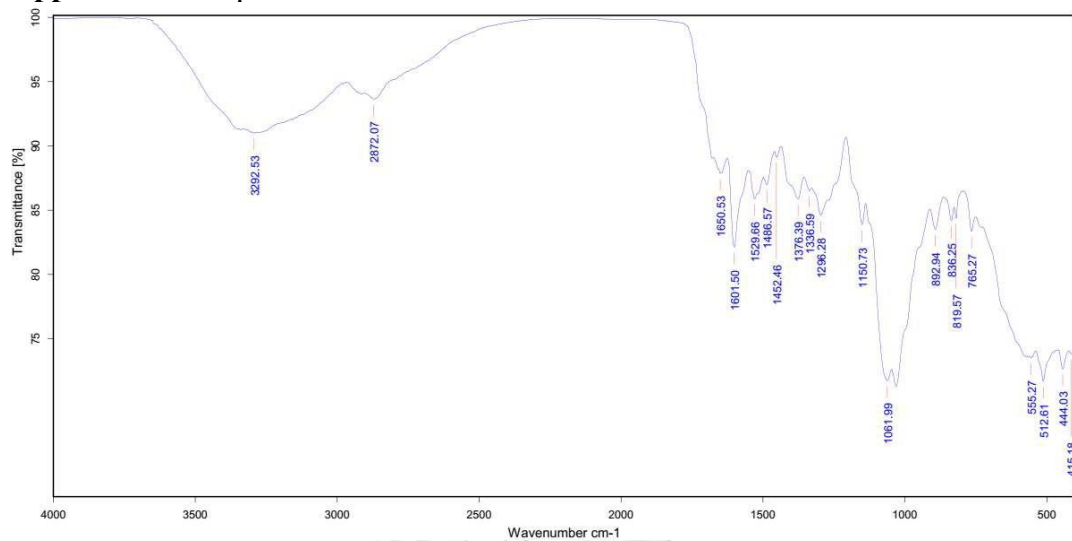
### Appendix 3. IR spectrum of FA

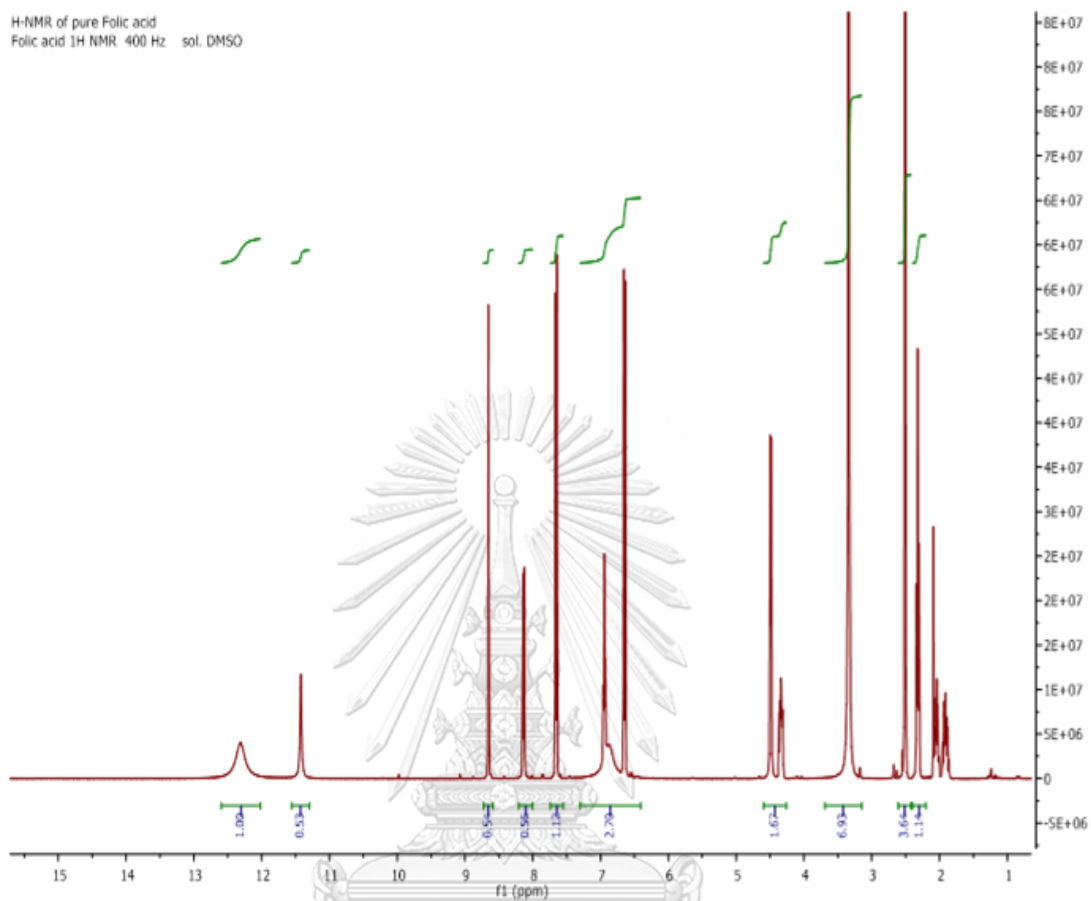


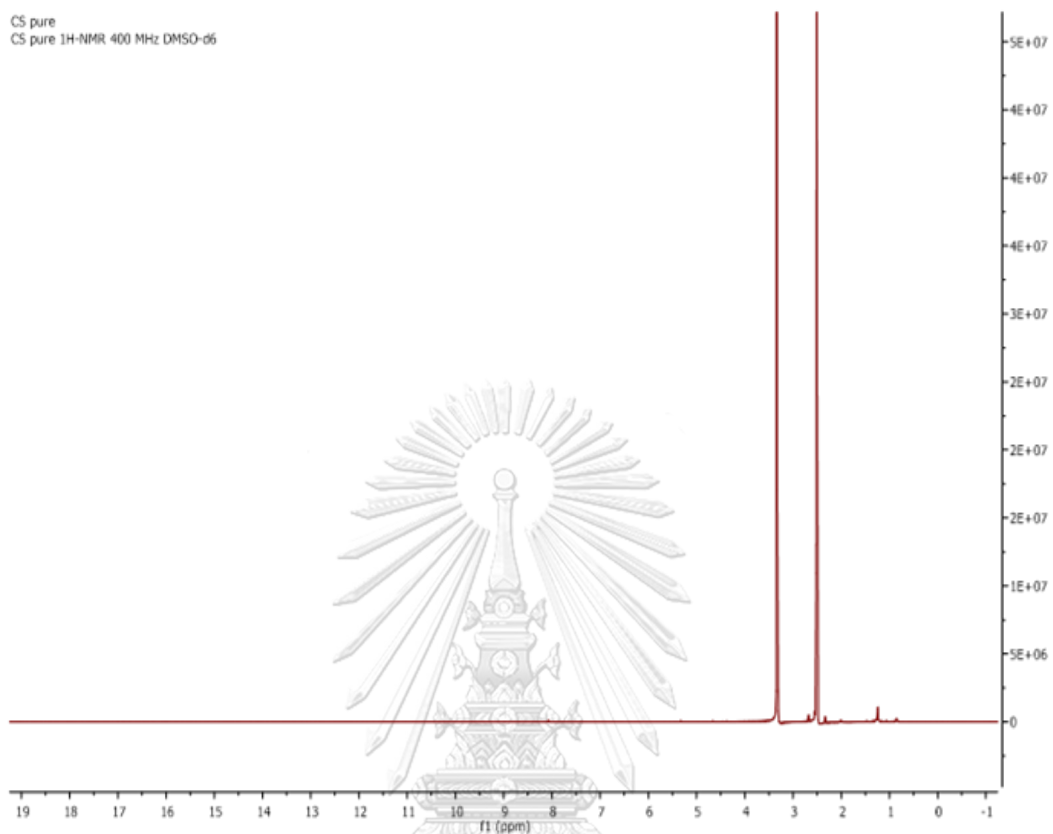
### Appendix 4. IR spectrum of CS



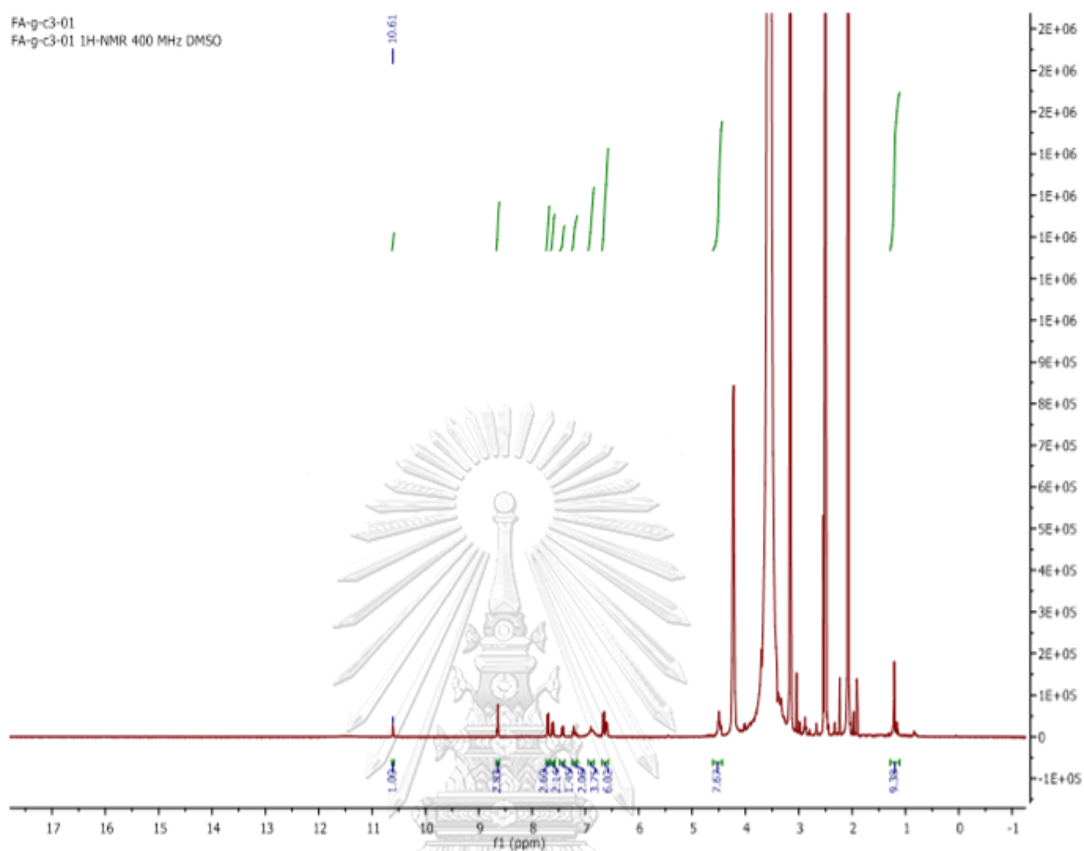


**Appendix 5. IR spectrum of FA-CS**

**Appendix 6.**  $^1\text{H}$ -NMR spectrum of FA

**Appendix 7.**  $^1\text{H-NMR}$  spectrum of CS

จุฬาลงกรณ์มหาวิทยาลัย  
CHULALONGKORN UNIVERSITY

**Appendix 8.**  $^1\text{H-NMR}$  spectrum of FA-CS

## REFERENCES



จุฬาลงกรณ์มหาวิทยาลัย  
**CHULALONGKORN UNIVERSITY**

1. Sung H, Ferlay J, Rebecca L, Siegel MPH, Laversanner M, Soerjomataram I, et al. Global cancer statistics 2020: globocan estimates of incidence and mortality worldwide for 36 cancers in 185 countries. *CA: Cancer J Clin.* 2021;71(3):209-249.
2. Lakha F, Suriyawongpaisul P, Sangrajang S, Leerapan B, Coker R. Breast cancer in Thailand: policy and health system challenges to universal healthcare. *Health Policy Plan.* 2020;35(9):1159-67.
3. Kumar P, Aggarwal R. An overview of triple-negative breast cancer. *Arch Gynecol Obstet.* 2016;293(2):247-69.
4. Medina MA, Oza G, Sharma A, Arriaga LG, Hernandez Hernandez JM, Rotello VM, et al. Triple-negative breast cancer: A review of conventional and advanced therapeutic strategies. *Int J Environ Res Public Health.* 2020;17(6):2078.
5. Vllasaliu D, Casettari L, Bonacucina G, Cespi M, Palmieri G, Illum L. Folic acid conjugated chitosan nanoparticles for tumor targeting of therapeutic and imaging agents. *Pharm Nanotechnol.* 2013;1:184-203.
6. Jain V, Kumar H, Anod HV, Chand P, Gupta NV, Dey S, et al. A review of nanotechnology-based approaches for breast cancer and triple-negative breast cancer. *J Control Release.* 2020;326:628-47.
7. Chanphai P, Konka V, Tajmir-Riahi HA. Folic acid-chitosan conjugation: A new drug delivery tool. *J. Mol. Liq.* 2017;238:155-9.
8. Sutradhar KB, Amin M. Nanotechnology in cancer drug delivery and selective targeting. *Int Sch Res Notices.* 2014;2014.
9. Prabakaran M. Review paper: chitosan derivatives as promising materials for controlled drug delivery. *J Biomater Appl.* 2008;23(1):5-36.
10. Prabhu RH, Patravale VB, Joshi MD. Polymeric nanoparticles for targeted treatment in oncology: current insights. *Int J Nanomedicine.* 2015;10:1001-18.
11. Lertsutthiwong P, Rojsitthisak P, Nimmannit U. Preparation of turmeric oil-loaded chitosan-alginate biopolymeric nanocapsules. *Mat Sci Eng C-Bio S.* 2009;29(3):856-60.
12. Lertsutthiwong P, Rojsitthisak P. Chitosan-alginate nanocapsules for encapsulation of turmeric oil. *Pharmazie.* 2011;66(12):911-5.
13. Lertsutthiwong P, Noomun K, Jongaroonngamsang N, Rojsitthisak P, Nimmannit U. Preparation of alginate nanocapsules containing turmeric oil. *Carbohydr Polym.* 2008;74(2):209-14.
14. Yao Y, Zhou Y, Liu L, Xu Y, Chen Q, Wang Y, et al. Nanoparticle-based drug delivery in cancer therapy and its role in overcoming drug resistance. *Front Mol Biosci.* 2020;7:193.
15. Chidambaram M, Manavalan R, Kathiresan K. Nanotherapeutics to overcome conventional cancer chemotherapy limitations. *J Pharm Pharm Sci.* 2011;14(1):67-77.
16. Kularatne SA, Low PS. Targeting of nanoparticles: folate receptor. *Cancer Nanotechnol.: Springer;* 2010. p. 249-65.
17. Paques JP, van der Linden E, van Rijn CJM, Sagis LMC. Preparation methods of alginate nanoparticles. *Adv Colloid Interface Sci.* 2014;209:163-71.
18. Barclay TG, Day CM, Petrovsky N, Garg S. Review of polysaccharide particle-

- based functional drug delivery. *Carbohydr. Polym.* 2019;221:94-112.
19. Yan F, Zhang C, Zheng Y, Mei L, Tang L, Song C, et al. The effect of poloxamer 188 on nanoparticle morphology, size, cancer cell uptake, and cytotoxicity. *Nanomed.: Nanotechnol. Biol. Med.* 2009;6:170-8.
  20. Bottari E, D'Ambrosio A, De Tommaso G, Festa MR, Iuliano M, Meschino M. Solubility of folic acid and protonation of folate in NaCl at different concentrations, even in physiological solution. *Analyst.* 2021;146(7):2339-47.
  21. Sambhi M, DeCarlo A, Malardier-Jugroot C, Szewczuk MR. Next-generation multimodality of nanomedicine therapy: size and structure dependence of folic acid conjugated copolymers actively target cancer cells in disabling cell division and inducing apoptosis. *Cancers (Basel).* 2019;11(11):1698.
  22. Pillai JJ, Thulasidasan AK, Anto RJ, Chithralekha DN, Narayanan A, Kumar GS. Folic acid conjugated cross-linked acrylic polymer (FA-CLAP) hydrogel for site specific delivery of hydrophobic drugs to cancer cells. *J Nanobiotechnology.* 2014;12:25.
  23. Pal K, Roy S, Parida PK, Dutta A, Bardhan S, Das S, et al. Folic acid conjugated curcumin loaded biopolymeric gum acacia microsphere for triple negative breast cancer therapy in invitro and invivo model. *Mater Sci Eng C Mater Biol Appl.* 2019;95:204-16.
  24. Mariadoss AVA, Saravanakumar K, Sathiyaseelan A, Venkatachalam K, Wang MH. Folic acid functionalized starch encapsulated green synthesized copper oxide nanoparticles for targeted drug delivery in breast cancer therapy. *Int J Biol Macromol.* 2020;164:2073-84.
  25. Cheng W, Nie J, Xu L, Liang C, Peng Y, Liu G, et al. pH-sensitive delivery vehicle based on folic acid-conjugated polydopamine-modified mesoporous silica nanoparticles for targeted cancer therapy. *ACS Appl Mater Interfaces.* 2017;9(22):18462-73.
  26. Natrajan D, Srinivasan S, Sundar K, Ravindran A. Formulation of essential oil-loaded chitosan-alginate nanocapsules. *J Food Drug Anal.* 2015;23(3):560-8.
  27. Danhier F, Feron O, Preat V. To exploit the tumor microenvironment: Passive and active tumor targeting of nanocarriers for anti-cancer drug delivery. *J Control Release.* 2010;148(2):135-46.
  28. Wahby S, Fashoyin-Aje L, Osgood CL, Cheng J, Fiero MH, Zhang L, et al. FDA approval summary: accelerated approval of sacituzumab govitecan-hziy for third-line treatment of metastatic triple-negative breast cancer. *Clin Cancer Res.* 2021;27(7):1850-4.
  29. Robert M, Patsouris A, Frenel JS, Gourmelon C, Augereau P, Campone M. Emerging PARP inhibitors for treating breast cancer. *Expert Opin Emerg Drugs.* 2018;23(3):211-21.
  30. Hoy SM. Talazoparib: first global approval. *Drugs.* 2018;78(18):1939-46.
  31. Reddy SM, Carroll E, Nanda R. Atezolizumab for the treatment of breast cancer. *Expert Rev Anticancer Ther.* 2020;20(3):151-8.
  32. Ducker GS, Rabinowitz JD. One-carbon metabolism in health and disease. *Cell Metab.* 2017;25(1):27-42.
  33. Rezvani M, Mohammadnejad J, Narmani A, Bidaki K. Synthesis and in vitro study of modified chitosan-polycaprolactam nanocomplex as delivery system. *Int. J. Biol. Macromol.* 2018;113:1287-93.

34. Storozhenko S, Ravanel S, Zhang GF, Rebeille F, Lambert W, Van Der Straeten D. Folate enhancement in staple crops by metabolic engineering. *Trends Food Sci Technol.* 2005;16(6-7):271-81.
35. Hilgenbrink AR, Low PS. Folate receptor-mediated drug targeting: from therapeutics to diagnostics. *J Pharm Sci.* 2005;94(10):2135-46.
36. Chen C, Ke J, Zhou XE, Yi W, Brunzelle JS, Li J, et al. Structural basis for molecular recognition of folic acid by folate receptors. *Nature.* 2013;500(7463):486-9.
37. Parker N, Turk MJ, Westrick E, Lewis JD, Low PS, Leamon CP. Folate receptor expression in carcinomas and normal tissues determined by a quantitative radioligand binding assay. *Anal Biochem.* 2005;338(2):284-93.
38. Ross JF, Chaudhuri PK, Ratnam M. Differential regulation of folate receptor isoforms in normal and malignant tissues in vivo and in established cell lines. Physiologic and clinical implications. *Cancer.* 1994;73(9):2432-43.
39. Paulos CM, Reddy JA, Leamon CP, Turk MJ, Low PS. Ligand binding and kinetics of folate receptor recycling in vivo: impact on receptor-mediated drug delivery. *Mol Pharmacol.* 2004;66(6):1406-14.
40. Larsen AK, Escargueil AE, Skladanowski A. Resistance mechanisms associated with altered intracellular distribution of anticancer agents. *Pharmacol Ther.* 2000;85(3):217-29.
41. Nair PR. Delivering combination chemotherapies and targeting oncogenic pathways via polymeric drug delivery systems. *Polymers (Basel).* 2019;11(4):630.
42. Wang H, Wang S, Liao Z, Zhao P, Su W, Niu R, et al. Folate-targeting magnetic core-shell nanocarriers for selective drug release and imaging. *Int J Pharm.* 2012;430(1-2):342-9.
43. Wang D, Chen W, Li H, Huang G, Zhou Y, Wang Y, et al. Folate-receptor mediated pH/reduction-responsive biomimetic nanoparticles for dually activated multi-stage anticancer drug delivery. *Int J Pharm.* 2020;585:119456.
44. Wileman T, Harding C, Stahl P. Receptor-mediated endocytosis. *Biochem J.* 1985;232(1):1-14.
45. Turek JJ, Leamon CP, Low PS. Endocytosis of folate-protein conjugates: ultrastructural localization in KB cells. *J Cell Sci.* 1993;106 ( Pt 1)(1):423-30.
46. Araujo MM, Marchioni E, Bergaentzle M, Zhao M, Kuntz F, Hahn E, et al. Irradiation stability of folic acid in powder and aqueous solution. *J Agric Food Chem.* 2011;59(4):1244-8.
47. Li P, Wang Y, Zeng F, Chen L, Peng Z, Kong LX. Synthesis and characterization of folate conjugated chitosan and cellular uptake of its nanoparticles in HT-29 cells. *Carbohydr Res.* 2011;346(6):801-6.
48. Zheng Y, Song X, Darby M, Liang Y, He L, Cai Z, et al. Preparation and characterization of folate-poly(ethylene glycol)-grafted-trimethylchitosan for intracellular transport of protein through folate receptor-mediated endocytosis. *J Biotechnol.* 2010;145(1):47-53.
49. Tan YL, Liu CG. Preparation and characterization of self-assembled nanoparticles based on folic acid modified carboxymethyl chitosan. *J Mater Sci-Mater M.* 2011;22(5):1213-20.
50. Jing H, Guo Z, Guo W, Yang W, Xu P, Zhang X. Synthesis and characterization



- of folic acid modified water-soluble chitosan derivatives for folate-receptor-mediated targeting. *Bioorg Med Chem Lett*. 2012;22(10):3418-24.
51. Qu D, Lin H, Zhang N, Xue J, Zhang C. In vitro evaluation on novel modified chitosan for targeted antitumor drug delivery. *Carbohydr Polym*. 2013;92(1):545-54.
  52. You J, Li X, de Cui F, Du YZ, Yuan H, Hu FQ. Folate-conjugated polymer micelles for active targeting to cancer cells: preparation, in vitro evaluation of targeting ability and cytotoxicity. *Nanotechnol*. 2008;19(4):045102.
  53. Wang FH, Zhang DR, Duan CX, Jia LJ, Feng FF, Liu Y, et al. Preparation and characterizations of a novel deoxycholic acid-O-carboxymethylated chitosan-folic acid conjugates and self-aggregates. *Carbohydr Polym*. 2011;84(3):1192-200.
  54. Wang F, Zhang D, Zhang Q, Chen Y, Zheng D, Hao L, et al. Synergistic effect of folate-mediated targeting and verapamil-mediated P-gp inhibition with paclitaxel -polymer micelles to overcome multi-drug resistance. *Biomaterials*. 2011;32(35):9444-56.
  55. Afzali E, Eslaminejad T, Yazdi Rouholamini SE, Shahrokhi-Farjah M, Ansari M. Cytotoxicity effects of curcumin loaded on chitosan alginate nanospheres on the KMBC-10 spheroids cell line. *Int J Nanomedicine*. 2021;16:579-89.
  56. Nejadshafiee V, Naeimi H, Goliaei B, Bigdeli B, Sadighi A, Dehghani S, et al. Magnetic bio-metal-organic framework nanocomposites decorated with folic acid conjugated chitosan as a promising biocompatible targeted theranostic system for cancer treatment. *Mater Sci Eng C*. 2019;99:805-15.
  57. Cheng LC, Jiang Y, Xie Y, Qiu LL, Yang Q, Lu HY. Novel amphiphilic folic acid-cholesterol-chitosan micelles for paclitaxel delivery. *Oncotarget*. 2017;8(2):3315-26.
  58. Li L, Liang N, Wang D, Yan P, Kawashima Y, Cui F, et al. Amphiphilic polymeric micelles based on deoxycholic acid and folic acid modified chitosan for the delivery of paclitaxel. *Int J Mol Sci*. 2018;19(10):3132.
  59. Bothiraja C, Rajput N, Poudel I, Rajalakshmi S, Panda B, Pawar A. Development of novel biofunctionalized chitosan decorated nanocochleates as a cancer targeted drug delivery platform. *Artif Cell Nanomed B*. 2018;46(sup1):S447-S61.
  60. Cheng L, Ma H, Shao M, Fan Q, Lv H, Peng J, et al. Synthesis of folate-chitosan nanoparticles loaded with ligustrazine to target folate receptor positive cancer cells. *Mol Med Rep*. 2017;16(2):1101-8.
  61. Sajjad M, Khan MI, Naveed S, Ijaz S, Qureshi OS, Raza SA, et al. Folate-functionalized thiomeric nanoparticles for enhanced docetaxel cytotoxicity and improved oral bioavailability. *AAPS PharmSciTech*. 2019;20(2):81.
  62. Esfandiarpour-Boroujeni S, Bagheri-Khoulenjani S, Mirzadeh H, Amanpour S. Fabrication and study of curcumin loaded nanoparticles based on folate-chitosan for breast cancer therapy application. *Carbohydr Polym*. 2017;168:14-21.
  63. Deb A, Andrews NG, Raghavan V. Natural polymer functionalized graphene oxide for co-delivery of anticancer drugs: In-vitro and in-vivo. *Int J Biol Macromol*. 2018;113:515-25.
  64. Yin L, Zhong Z. *Nanoparticles*. *Biomaterials Science*: Elsevier; 2020. p. 453-

- 84.
65. Schäfer-Korting M. Drug delivery: Springer Science & Business Media; 2010.
66. Yu L, Dean K, Li L. Polymer blends and composites from renewable resources. *Prog Polym Sci.* 2006;31(6):576-602.
67. Chellat F, Merhi Y, Moreau A, Yahia L. Therapeutic potential of nanoparticulate systems for macrophage targeting. *Biomaterials.* 2005;26(35):7260-75.
68. Coppi G, Iannuccelli V. Alginate/chitosan microparticles for tamoxifen delivery to the lymphatic system. *Int J Pharm.* 2009;367(1-2):127-32.
69. Jayakumar R, Menon D, Manzoor K, Nair SV, Tamura H. Biomedical applications of chitin and chitosan based nanomaterials-A short review. *Carbohydr. Polym.* 2010;82(2):227-32.
70. Shukla RK, Tiwari A. Carbohydrate polymers: Applications and recent advances in delivering drugs to the colon. *Carbohydr. Polym.* 2012;88(2):399-416.
71. Agüero L, Zaldivar-Silva D, Peña L, Dias ML. Alginate microparticles as oral colon drug delivery device: A review. *Carbohydr. Polym.* 2017;168:32-43.
72. Pawar SN, Edgar KJ. Alginate derivatization: a review of chemistry, properties and applications. *Biomaterials.* 2012;33(11):3279-305.
73. Mohammed A, Bissoon R, Bajnath E, Mohammed K, Lee T, Bissram M, et al. Multistage extraction and purification of waste *Sargassum natans* to produce sodium alginate: An optimization approach. *Carbohydr. Polym.* 2018;198:109-18.
74. Goh CH, Heng PWS, Chan LW. Alginates as a useful natural polymer for microencapsulation and therapeutic applications. *Carbohydr. Polym.* 2012;88(1):1-12.
75. Draget KI, Skjak-Braek G, Smidsrod O. Alginate based new materials. *Int J Biol Macromol.* 1997;21(1-2):47-55.
76. Yang S-J, Lin F-H, Tsai H-M, Lin C-F, Chin H-C, Wong J-M, et al. Alginate-folic acid-modified chitosan nanoparticles for photodynamic detection of intestinal neoplasms. *Biomaterials.* 2011;32(8):2174-82.
77. Li J, He J, Huang Y. Role of alginate in antibacterial finishing of textiles. *Int J Biol Macromol.* 2017;94(Pt A):466-73.
78. Dalheim MO, Vanacker J, Najmi MA, Aachmann FL, Strand BL, Christensen BE. Efficient functionalization of alginate biomaterials. *Biomaterials.* 2016;80:146-56.
79. Tonnesen HH, Karlsen J. Alginate in drug delivery systems. *Drug Dev Ind Pharm.* 2002;28(6):621-30.
80. Phillips G, Williams P, Wedlock D. Gums and stabilizers for the food industry 5: Applications of alginates. New York: IRL Press at Oxford University Press; 1990.
81. De S, Robinson D. Polymer relationships during preparation of chitosan-alginate and poly-l-lysine-alginate nanospheres. *J Control Release.* 2003;89(1):101-12.
82. Mallikarjuna SC, Sahoo SS, Sa B. Alginate-coated alginate-polyethyleneimine beads for prolonged release of furosemide in simulated intestinal fluid. *Drug Dev Ind Pharm.* 2005;31(4-5):435-46.

83. Motiei M, Kashanian S, Lucia LA, Khazaei M. Intrinsic parameters for the synthesis and tuned properties of amphiphilic chitosan drug delivery nanocarriers. *J. Control Release*. 2017;260:213-25.
84. Yuan Y, Chesnutt BM, Haggard WO, Bumgardner JD. Deacetylation of Chitosan: Material characterization and *in vitro* evaluation via albumin adsorption and pre-osteoblastic cell cultures. *Materials (Basel)*. 2011;4(8):1399-416.
85. George M, Abraham TE. Polyionic hydrocolloids for the intestinal delivery of protein drugs: alginate and chitosan--a review. *J. Control Release*. 2006;114(1):1-14.
86. Xiao B, Chen Q, Zhang Z, Wang L, Kang Y, Denning T, et al. TNFalpha gene silencing mediated by orally targeted nanoparticles combined with interleukin-22 for synergistic combination therapy of ulcerative colitis. *J. Control Release*. 2018;287:235-46.
87. Yan Q, Chen X, Gong H, Qiu P, Xiao X, Dang S, et al. Delivery of a TNF-alpha-derived peptide by nanoparticles enhances its antitumor activity by inducing cell-cycle arrest and caspase-dependent apoptosis. *FASEB J*. 2018;32(12):fj201800377R.
88. Martínez-Martínez M, Rodríguez-Berna G, Gonzalez-Alvarez I, Hernández MaJs, Corma A, Bermejo M, et al. Ionic hydrogel based on chitosan cross-linked with 6-phosphogluconic trisodium salt as a drug delivery system. *Biomacromol*. 2018;19(4):1294-304.
89. Ali A, Ahmed S. A review on chitosan and its nanocomposites in drug delivery. *Int J Biol Macromol*. 2018;109:273-86.
90. Das RK, Kasoju N, Bora U. Encapsulation of curcumin in alginate-chitosan-pluronic composite nanoparticles for delivery to cancer cells. *Nanomedicine*. 2010;6(1):153-60.
91. Li P, Dai YN, Zhang JP, Wang AQ, Wei Q. Chitosan-alginate nanoparticles as a novel drug delivery system for nifedipine. *Int J Biomed Sci* 2008;4(3):221.
92. Song H, Su C, Cui W, Zhu B, Liu L, Chen Z, et al. Folic acid-chitosan conjugated nanoparticles for improving tumor-targeted drug delivery. *Biomed Res Int*. 2013;2013:723158.
93. Gopinath H, Karthikeyan K. Turmeric: A condiment, cosmetic and cure. *Indian J Dermatol Venereol Leprol*. 2018;84(1):16-21.
94. Debjit BC, Kumar KS, Chandira M, Jayakar B. Turmeric: a herbal and traditional medicine. *Arch Appl Sci Res*. 2009;1(2):86-108.
95. Niranjana A, Prakash D. Chemical constituents and biological activities of turmeric (*Curcuma longa* L.) - A review. *J Food Sci Technol* 2008;45(2):109-16.
96. Leela NK, Tava A, Shafi PM, John SP, Chempakam B. Chemical composition of essential oils of turmeric (*Curcuma longa* L.). *Acta Pharm Sin B*. 2002;52(2):137-4.
97. Dosoky NS, Setzer WN. Chemical composition and biological activities of essential oils of curcuma species. *Nutrients*. 2018;10(9):1196.
98. He XG, Lin LZ, Lian LZ, Lindenmaier M. Liquid chromatography electrospray mass spectrometric analysis of curcuminoids and sesquiterpenoids in turmeric (*Curcuma longa*). *J Chromatogr A*. 1998;818(1):127-32.

99. Liao JC, Tsai JC, Liu CY, Huang HC, Wu LY, Peng WH. Antidepressant-like activity of turmerone in behavioral despair tests in mice. *BMC Complement Altern Med.* 2013;13(1):299.
100. Orellana-Paucar AM, Afrikanova T, Thomas J, Aibuldinov YK, Dehaen W, de Witte PAM, et al. Insights from zebrafish and mouse models on the activity and safety of *ar*-turmerone as a potential drug candidate for the treatment of epilepsy. *Plos One.* 2013;8(12):e81634.
101. Jankasem M, Wuthi-Udomlert M, Gritsanapan W. Antidermatophytic properties of *ar*-turmerone, turmeric oil, and *Curcuma longa* preparations. *ISRN Dermatol.* 2013;2013:250597.
102. Nishiyama T, Mae T, Kishida H, Tsukagawa M, Mimaki Y, Kuroda M, et al. Curcuminoids and sesquiterpenoids in turmeric (*Curcuma longa* L.) suppress an increase in blood glucose level in type 2 diabetic KK-Ay mice. *J Agric Food Chem.* 2005;53(4):959-63.
103. Lee HS. Antiplatelet property of *Curcuma longa* L. rhizome-derived *ar*-turmerone. *Bioresour Technol.* 2006;97(12):1372-6.
104. Apisariyakul A, Vanittanakom N, Buddhasukh D. Antifungal activity of turmeric oil extracted from *Curcuma longa* (Zingiberaceae). *J Ethnopharmacol.* 1995;49(3):163-9.
105. Negi PS, Jayaprakasha GK, Jagan Mohan Rao L, Sakariah KK. Antibacterial activity of turmeric oil: a byproduct from curcumin manufacture. *J Agric Food Chem.* 1999;47(10):4297-300.
106. Roth GN, Chandra A, Nair MG. Novel bioactivities of *Curcuma longa* constituents. *J Nat Prod.* 1998;61(4):542-5.
107. Jayaprakasha GK, Jena BS, Negi PS, Sakariah KK. Evaluation of antioxidant activities and antimutagenicity of turmeric oil: a byproduct from curcumin production. *J. Biosci.* 2002;57(9-10):828-35.
108. Aratanechemuge Y, Komiya T, Moteki H, Katsuzaki H, Imai K, Hibasami H. Selective induction of apoptosis by *ar*-turmerone isolated from turmeric (*Curcuma longa* L) in two human leukemia cell lines, but not in human stomach cancer cell line. *Int J Mol Med.* 2002;9(5):481-4.
109. Yue GGL, Chan BCL, Hon P-M, Lee MYH, Fung K-P, Leung P-C, et al. Evaluation of in vitro anti-proliferative and immunomodulatory activities of compounds isolated from *Curcuma longa*. *Food Chem Toxicol.* 2010;48(8):2011-20.
110. Alupe L, Lisa G, Butnariu A, Desbrieres J, Cadinoiu AN, Peptu CA, et al. New folic acid-chitosan derivative based nanoparticles - potential applications in cancer therapy. *Cellul Chem Technol.* 2017;51(7-8):631-48.
111. Rajkumar V, Gunasekaran C, Paul CA, Dharmaraj J. Development of encapsulated peppermint essential oil in chitosan nanoparticles: characterization and biological efficacy against stored-grain pest control. *Pestic Biochem Phys.* 2020;170:104679.
112. Panwar P, Pandey B, Lakhera PC, Singh KP. Preparation, characterization, and in vitro release study of albendazole-encapsulated nanosize liposomes. *Int J Nanomedicine.* 2010;5:101-8.
113. Acharya SR, Reddy PRV. Brain targeted delivery of paclitaxel using endogenous ligand. *Asian J Pharm Sci.* 2016;11(3):427-38.

114. Sorasitthiyankarn FN, Muangnoi C, Rojsitthisak P, Rojsitthisak P. Chitosan-alginate nanoparticles as effective oral carriers to improve the stability, bioavailability, and cytotoxicity of curcumin diethyl disuccinate. *Carbohydr. Polym.* 2021;256:117426.
115. Yang S-J, Lin F-H, Tsai K-C, Wei M-F, Tsai H-M, Wong J-M, et al. Folic acid-conjugated chitosan nanoparticles enhanced protoporphyrin IX accumulation in colorectal cancer cells. *Bioconjug Chem.* 2010;21(4):679-89.
116. Viswanadh MK, Mehata AK, Sharma V, Priya V, Varshney N, Mahto SK, et al. Bioadhesive chitosan nanoparticles: dual targeting and pharmacokinetic aspects for advanced lung cancer treatment. *Carbohydr. Polym.* 2021;274:118617.
117. Ji J, Wu D, Liu L, Chen J, Xu Y. Preparation, characterization, and in vitro release of folic acid-conjugated chitosan nanoparticles loaded with methotrexate for targeted delivery. *Polymer Bulletin.* 2012;68(6):1707-1720.
118. Mehrotra N, Sabarinath S, Suryawanshi S, Raj K, Gupta RC. LC–UV assay for simultaneous estimation of aromatic turmerone,  $\alpha/\beta$ -turmerone and curcumin: major bisabolane sesquiterpenes of turmeric oil in rabbit plasma for application to pharmacokinetic studies. *Chromatographia.* 2009;69(9):1077-82.
119. Loquercio A, Castell-Perez E, Gomes C, Moreira RG. Preparation of chitosan-alginate nanoparticles for trans-cinnamaldehyde entrapment. *J Food Sci.* 2015;80(10):N2305-15.
120. Bolla PK, Gote V, Singh M, Yellepeddi VK, Patel M, Pal D, et al. Preparation and characterization of lutein loaded folate conjugated polymeric nanoparticles. *J Microencapsul.* 2020;37(7):502-16.
121. Caracciolo G. Clinically approved liposomal nanomedicines: lessons learned from the biomolecular corona. *Nanoscale.* 2018;10(9):4167-72.
122. Afzali E, Eslaminejad T, Rouholamini SEY, Shahrokhi-Farjah M, Ansari M. Cytotoxicity effects of curcumin loaded on chitosan alginate nanospheres on the KMBC-10 spheroids cell line. *Int J Nanomedicine.* 2021;16:579.
123. Sorasitthiyankarn FN, Muangnoi C, Ratnatilaka Na Bhuket P, Rojsitthisak P, Rojsitthisak P. Chitosan/alginate nanoparticles as a promising approach for oral delivery of curcumin diglutaric acid for cancer treatment. *Mater Sci Eng C.* 2018;93:178-90.
124. Manaspon C, Viravaidya-Pasuwat K, Pimpha N. Preparation of folate-conjugated pluronic F127/chitosan core-shell nanoparticles encapsulating doxorubicin for breast cancer treatment. *J Nanomater.* 2012;11:593878.
125. Sorasitthiyankarn FN, Ratnatilaka Na Bhuket P, Muangnoi C, Rojsitthisak P, Rojsitthisak P. Chitosan/alginate nanoparticles as a promising carrier of novel curcumin diethyl diglutarate. *Int J Biol Macromol.* 2019;131:1125-36.
126. Fattahpour S, Shamanian M, Tavakoli N, Fathi M, Sheykhi SR, Fattahpour S. Design and optimization of alginate-chitosan-pluronic nanoparticles as a novel meloxicam drug delivery system. *J Appl Polym Sci.* 2015;132(28).
127. Augustine R, Hasan A. Cellular response to nanobiomaterials. *Handbook of biomaterials biocompatibility*: Elsevier; 2020. p. 473-504.
128. Bhunchu S, Rojsitthisak P, Rojsitthisak P. Effects of preparation parameters on the characteristics of chitosan–alginate nanoparticles containing curcumin diethyl disuccinate. *J Drug Deliv Sci Technol.* 2015;28:64-72.

129. Lopes MA, Abraham-Vieira B, Oliveira C, Fonte P, Souza AMT, Lira T, et al. Probing insulin bioactivity in oral nanoparticles produced by ultrasonication-assisted emulsification/internal gelation. *Int J Nanomedicine*. 2015; 10:5865-80.
130. Sorasitthiyankarn FN, Ratnatilaka Na Bhuket P, Muangnoi C, Rojsitthisak P, Rojsitthisak P. Chitosan/alginate nanoparticles as a promising carrier of novel curcumin diethyl diglutarate. *Int J Biol Macromol*. 2019;131:1125-36.
131. Wang F, Yang S, Yuan J, Gao Q, Huang C. Effective method of chitosan-coated alginate nanoparticles for target drug delivery applications. *J Biomater Appl*. 2016;31(1):3-12.
132. El Leithy ES, Abdel-Bar HM, Ali RA. Folate-chitosan nanoparticles triggered insulin cellular uptake and improved in vivo hypoglycemic activity. *Int J Pharm*. 2019;571:118708.
133. Sorasitthiyankarn FN, Muangnoi C, Rojsitthisak P, Rojsitthisak P. Chitosan oligosaccharide/alginate nanoparticles as an effective carrier for astaxanthin with improving stability, in vitro oral bioaccessibility, and bioavailability. *Food Hydrocoll*. 2022;124:107246.
134. Bolla PK, Gote V, Singh M, Yellepeddi VK, Patel M, Pal D, et al. Preparation and characterization of lutein loaded folate conjugated polymeric nanoparticles. *J Microencapsul*. 2020; 37(7):502-516.
135. Yan F, Zhang C, Zheng Y, Mei L, Tang L, Song C, Sun H, Huang L. The effect of poloxamer 188 on nanoparticle morphology, size, cancer cell uptake, and cytotoxicity. *Nanomed.: Nanotechnol. Biol. Med*. 2010;6(1):170-178.

## VITA

**NAME** Ms. Htet Htet Moe San

**DATE OF BIRTH** 17 July 1995

**PLACE OF BIRTH** Yangon, Myanmar

**INSTITUTIONS ATTENDED** University of Pharmacy (Yangon)

**HOME ADDRESS** Yangon, Myanmar

**AWARD RECEIVED** 2020-2021 CU-ASEAN/NON- ASEAN Scholarship from Chulalongkorn University, Thailand



จุฬาลงกรณ์มหาวิทยาลัย  
CHULALONGKORN UNIVERSITY